

# FURTHER-FC Newsletter #6

## Further Understanding Related to Transport limitations at High current density towards future Electrodes for Fuel Cells

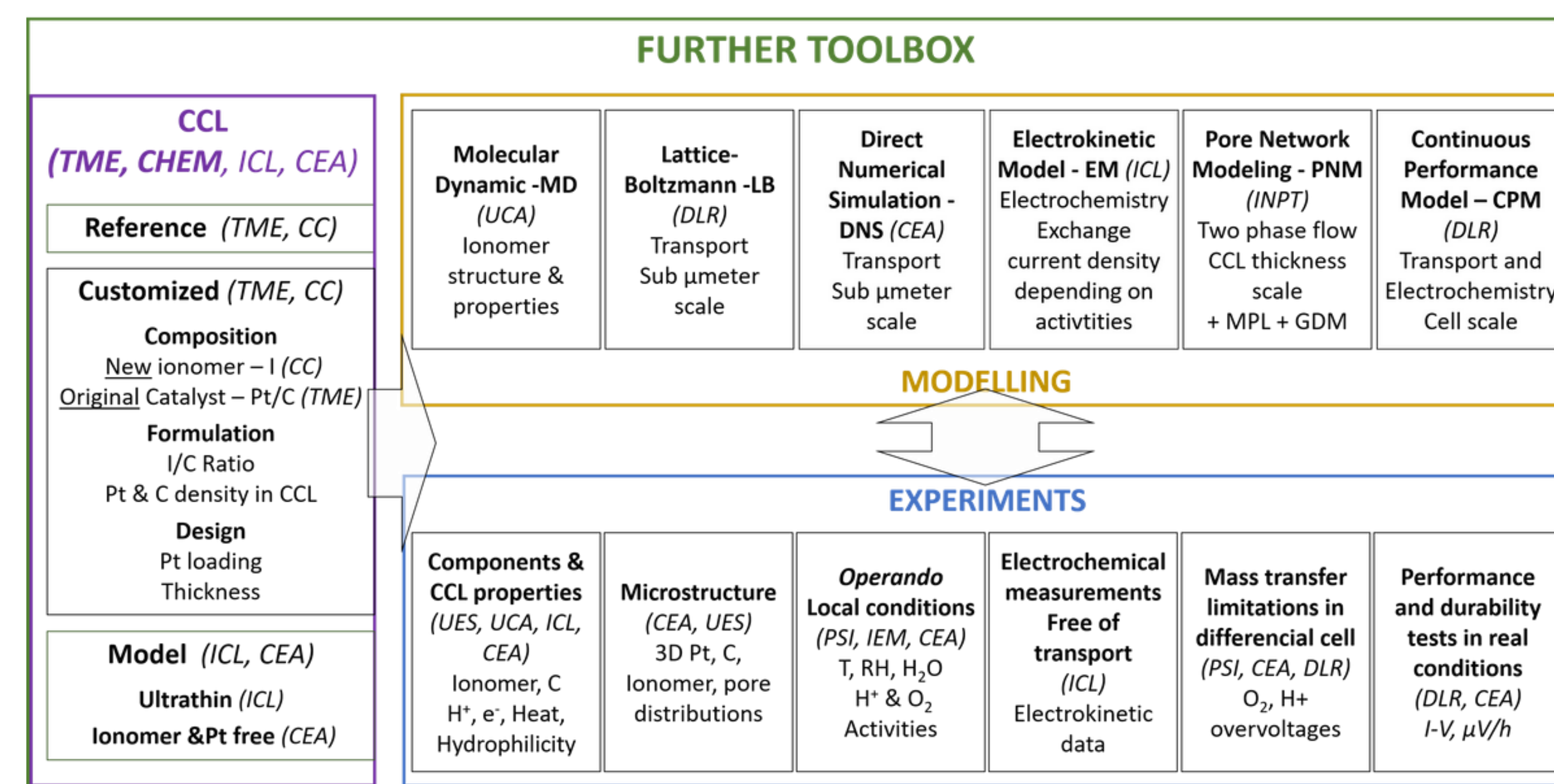


### Project aim

The final objective of the EU-Project FURTHER-FC is to support and promote the manufacturing and deployment of fuel cell vehicles, through the specification and design of better performing and more durable Membrane Electrode Assembly (MEA) as core and critical component for the electrochemical conversion in Polymer Electrolyte Fuel Cells (PEMFCs).

<https://further-fc.eu/>

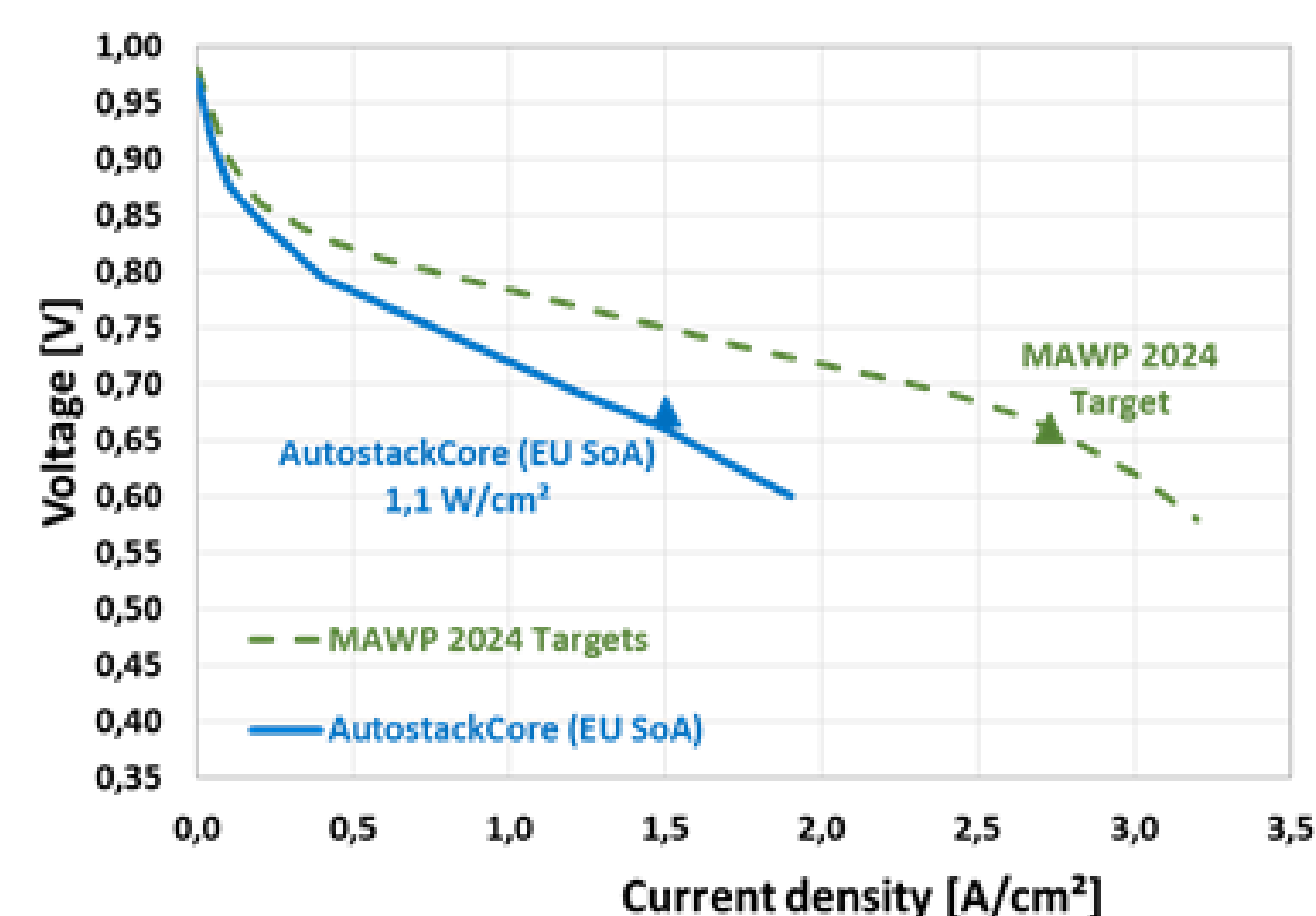
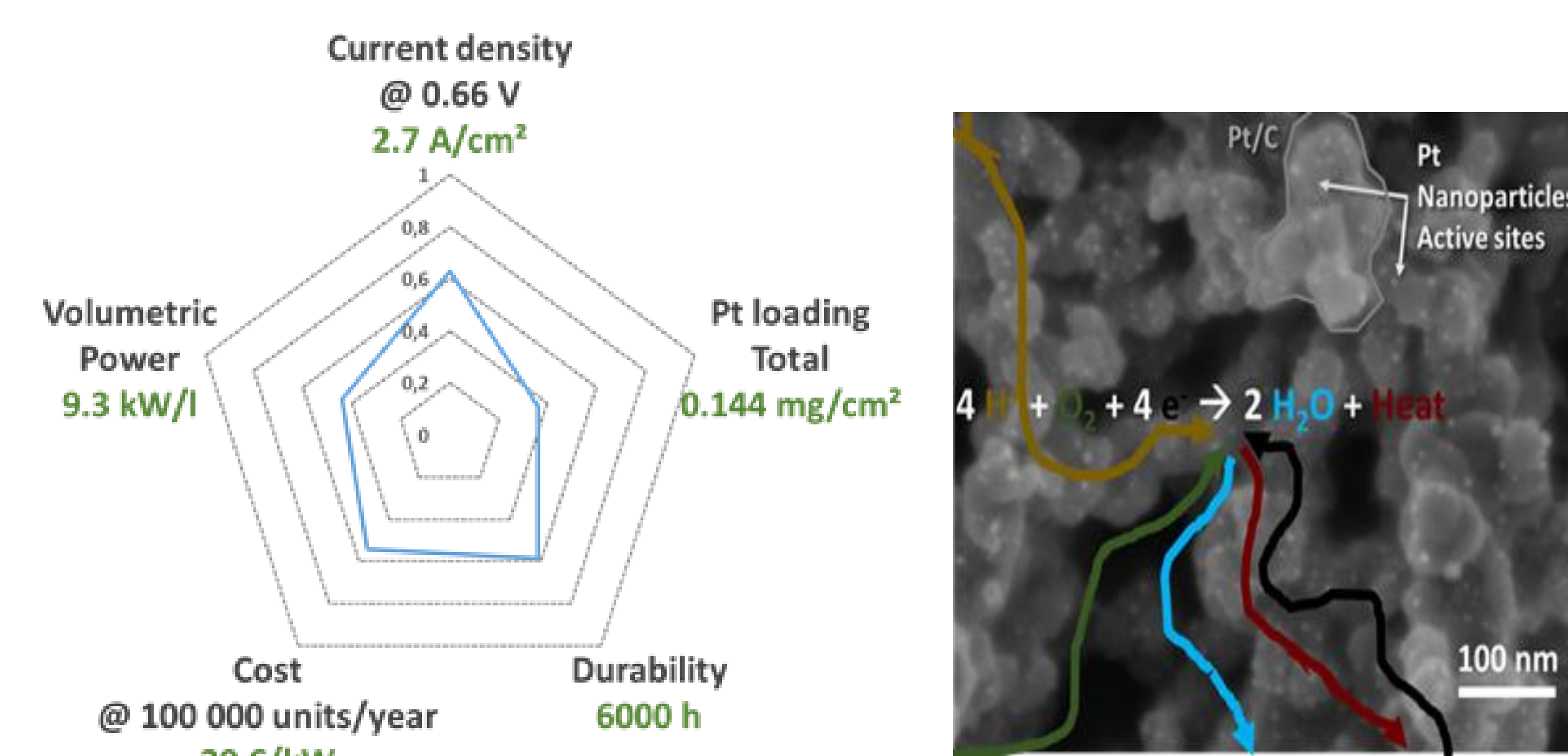
### FURTHER-FC TOOLBOX



## Project summary

### Introduction

Fuel cells, as a highly efficient energy conversion technology, and hydrogen, as a clean energy carrier, have a great potential to reduce both carbon dioxide emissions and dependence on mainly imported hydrocarbons. Fuel cells and Hydrogen are expected to become major contributors to a competitive economic growth in Europe as well for energy stationary applications as for transportation. Currently, Proton Exchange Membrane Fuel Cells (PEMFC) cars –Toyota Mirai, Honda Clarity, and Hyundai Nexa - are commercially available with reasonable cost despite a crude production. Compared to the electric vehicles powered by batteries, the fuel cell vehicles offer a shorter refueling time of a few minutes. In addition, owing to the use of a solid electrolyte and to quicker and safer disassembling and materials-separation processes the PEMFC are much more easily recycled than lithium batteries. Therefore, PEMFC is the predilection technology for transportation applications with a large deployment horizon by 2025-2030, especially for heavy duty transportation. The Fuel Cell Systems analysis for automotive applications presented by Strategic Analysis Inc. during the 2017 DOE Hydrogen and Fuel Cells Program Review clearly shows the strategic importance to increase power density while simultaneously decreasing all component costs, and especially via the reduction of Pt loading. This conclusion is fully consistent with the priorities defined for horizon 2024 in the Multi Annual Work Plan (MAWP) of the FCH-JU, stating that the next generation PEMFC stack for light duty vehicles including cars requests to operate at high current densities ( $>2.7 \text{ A/cm}^2$ ), high power densities ( $1.8 \text{ W/cm}^2$ ,  $9.3 \text{ kW/l}$ ,  $0.08 \text{ gPt/kW}$ ) with low PGM catalyst total loading ( $<0.144 \text{ mg/cm}^2$ ), with high durability ( $>6,000\text{h}$  with 10% loss of performance) and low cost ( $<50 \text{ €/kW}$ ). The current status (for instance AutoStackCore4 project) is still far from these targets reaching approximatively  $1.13 \text{ W/cm}^2$ ,  $4.1 \text{ kW/l}$  and durability of 3,000 hours with 20-25  $\mu\text{V/h}$  voltage loss at nominal point  $1.5\text{A/cm}^2$  (FC-DLC durability tests, Fuel Cell-Drive Load Cycle), for approx.  $0.4 \text{ mg PGM/cm}^2$  (e.g.  $0.35 \text{ g/kW}$  at BoL)



INDICATORS	EU SoA 2018 <sup>2</sup>	Targets MAWP 2024
Cell volumetric power (kW/l)	4.1	9.3
Power density (W/cm²)	1.13	>1.8
Cost (€/kW) at 100 000 units/year	36.8	< 20
Durability (hours)	3,500	6,000
Total Pt loading (mg/cm²)	0.4	0.144
Total Pt loading (g/kW)	0.35	0.08
Pt efficiency @0.66 V (A/mg)	4.5	15

It is obvious that filling the gap between State-of-the-Art and FCH-JU 2030 targets, will not be possible by incremental, or trial and error approaches. It is unanimously admitted that R&D efforts have to be focused on the Membrane Electrode Assembly (MEA), where the electrochemical conversion takes place thanks to platinum, to reach these objectives. Indeed, the MEA is at the heart of the PEMFC stack and is the most costly component, representing about 60% of the cost of the stack (i.e. 30% of the total cost of the system for which the stack represents 50%<sup>2</sup>) The Cathode Catalyst Layer (CCL), where the conversion of  $2 \text{ O}_2$  with 4 protons and 4 electrons into  $\text{H}_2\text{O}$  occurs onto the active sites of Pt nanoparticles via the Oxidation Reduction Reaction (ORR), can represent about 31% of the total cost of the stacks. In addition, up to 70% of the total performance limitations are due to the complex coupling, occurring within the CCL, between the sluggish ORR kinetic and the transport phenomena which limits the Pt utilization and effectiveness (Figure 2). Finally, because Pt based catalyst is prone to degradation, whose extent and consequence depends on the critical role of the transport phenomena, CCL becomes the major limiting component considering PEMFC durability. This negative combination of high cost, lack of stability and low efficiency explains why reducing the Pt content in the CCL meanwhile looking for its highest utilization by reducing transport losses, is mandatory to achieve the Fuel Cell and Hydrogen Joint Undertakings (FCH-JU) 2024 targets.

# FURTHER-FC Newsletter #6

## Further Understanding Related to Transport limitations at High current density towards future ElectRodes for Fuel Cells



### Project overview

#### Objectives

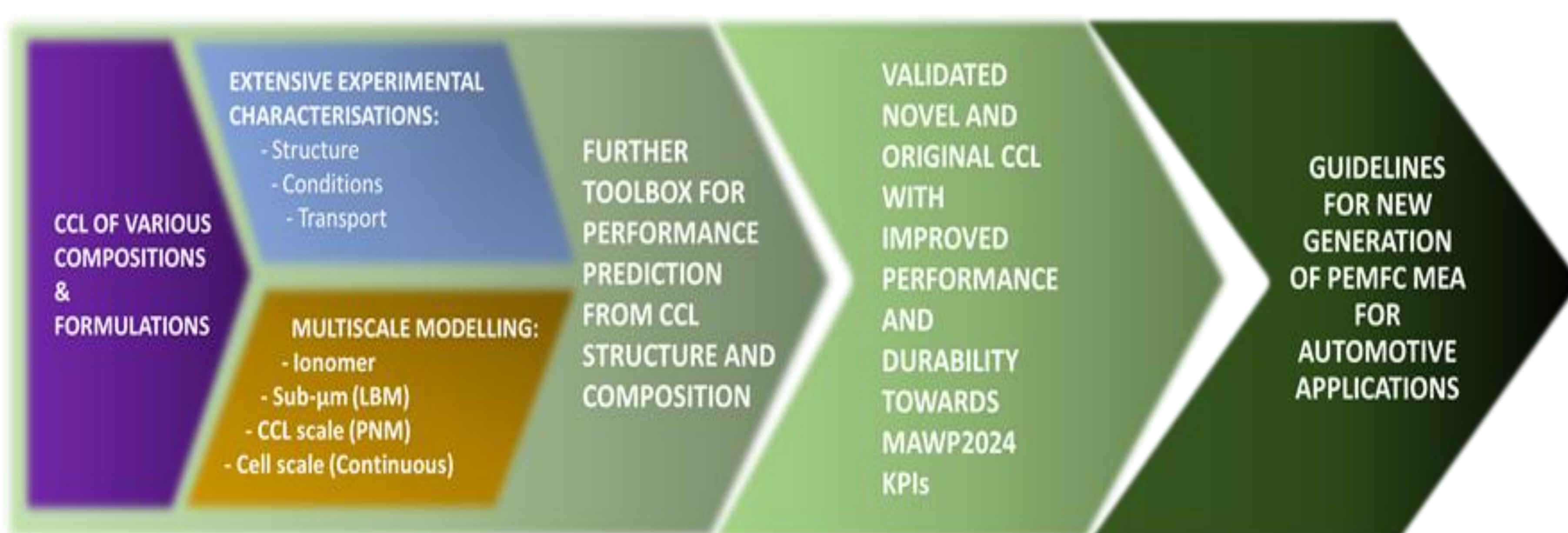
#### Concept

The FURTHER-FC project aims at understanding performance limitations due to the coupling between electrochemical and transport issues in the Cathode Catalyst Layer (CCL) which is the main bottleneck for future PEMFC.

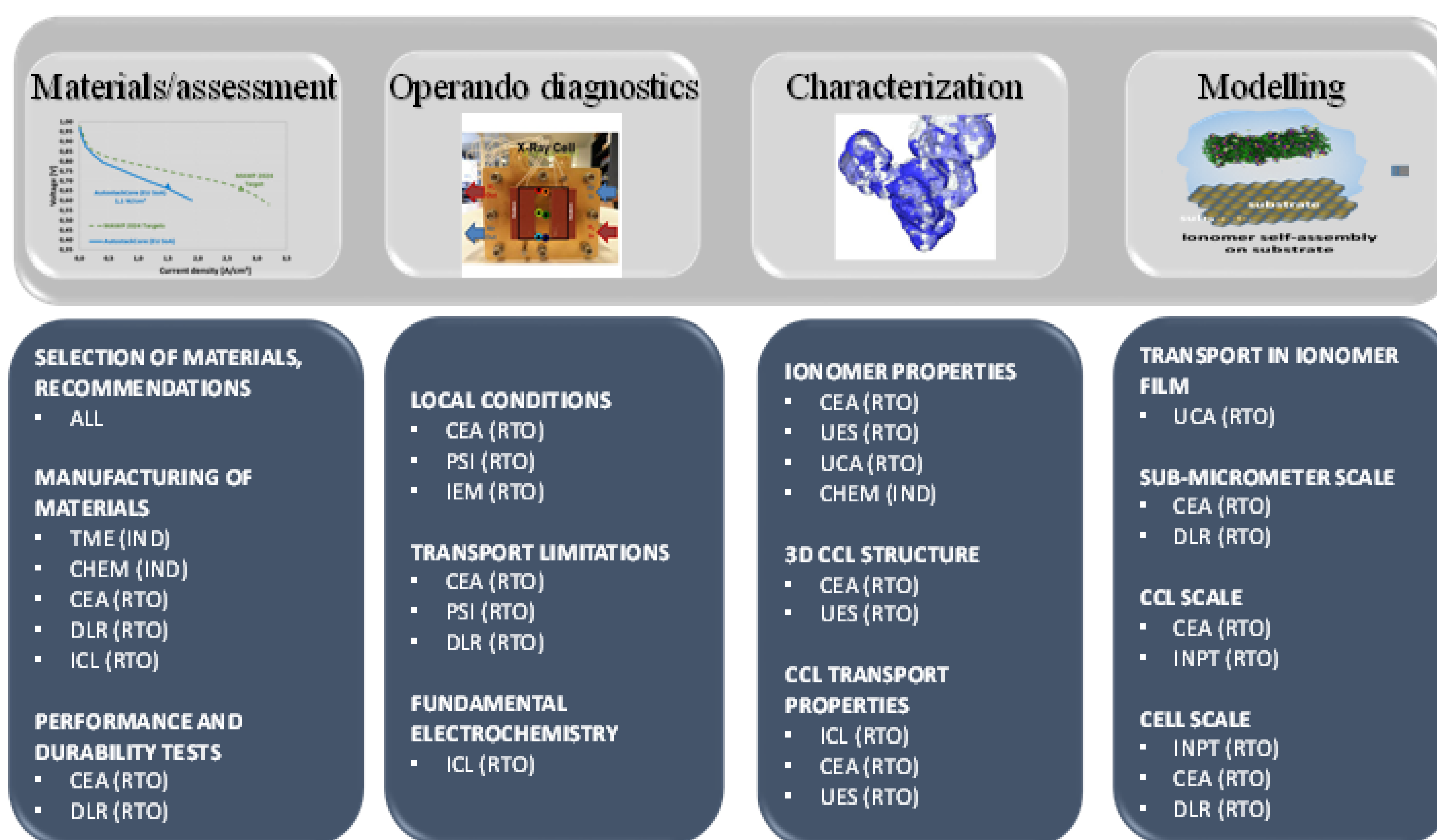
More precisely, the main objectives are to:

- Describe the cathode catalyst layer (CCL) structure and transport properties and mechanisms at its different scales
- Characterize of the local conditions in the CCL during operation
- Establish the link between structure / properties of CCL, local conditions during operation, and performance
- Propose and validate the performance and durability new ionomer and electrode structures specifically designed to prevent the limitations observed on current MEA, contributing to reach the MAWP targets for HORIZON 2024-2030.

FURTHER-FC proposes a **complete experimental and modelling coupled platform** to be able to **predict performance** of MEA based on the **knowledge of CCL composition and morphology**. The concept starts from the **design and the manufacturing of CCL customized in the composition** to be intensively studied with the platforms. The resulting knowledge and tools will be used as a **toolbox to design a CCL made with original and novel materials (ionomer and catalyst)** in the view of manufacturing a **MEA with improved performance and durability** to go towards the KPIs of the 2024 MAWP



### Role of each partner



## Results

The table below shows the list of material and the composition of the reference MEA. Materials and composition were selected based on state-of-the-art for automotive applications. As GDL, we selected the Sigracet 22BB from SGL (Germany). It is specifically designed for Automotive application with a thickness of 215 µm. The GDL is already prepared with PTFE (5%) and with a MPL layer on one side. Membrane and ionomer are supplied by Chemours (Project partner). We selected the NC700 as the membrane whose thickness is 15 µm with a reinforcement layer. D2020CS (20% Nafion® dispersion) is selected as ionomer for the cathode and anode catalyst layer. The reference catalyst is supplied by Tanaka Kikinzoku. We selected the TEC10E50E (46.2 wt% Pt on high surface area carbon) which is a state-of-the-art material in the PEMFC community. Based on state-of-the-art and internal knowledge in TME, the ionomer/carbon (I/C) weight ratio is set to 0.8. Regarding catalyst loading, cathode amount is set to 0.2 mg<sub>Pt</sub>/cm<sup>2</sup> and anode is set to 0.1 mg<sub>Pt</sub>/cm<sup>2</sup>.

#### Project Reference MEA

	Cathode	Anode
GDL	Sigracet 22BB (SGL)	
Membrane	NC700 (Chemours)	
Catalyst	TEC10E50E 46.2% Pt on High surface area carbon (Tanaka)	
Ionomer	D2020CS / 20% Nafion dispersion (Chemours)	
I / C weight ratio	0.8	
Loading	0.2 mg <sub>Pt</sub> /cm <sup>2</sup>	0.1 mg <sub>Pt</sub> /cm <sup>2</sup>

# FURTHER-FC Newsletter #6

## Further Understanding Related to Transport limitations at High current density towards future ElectRodes for Fuel Cells

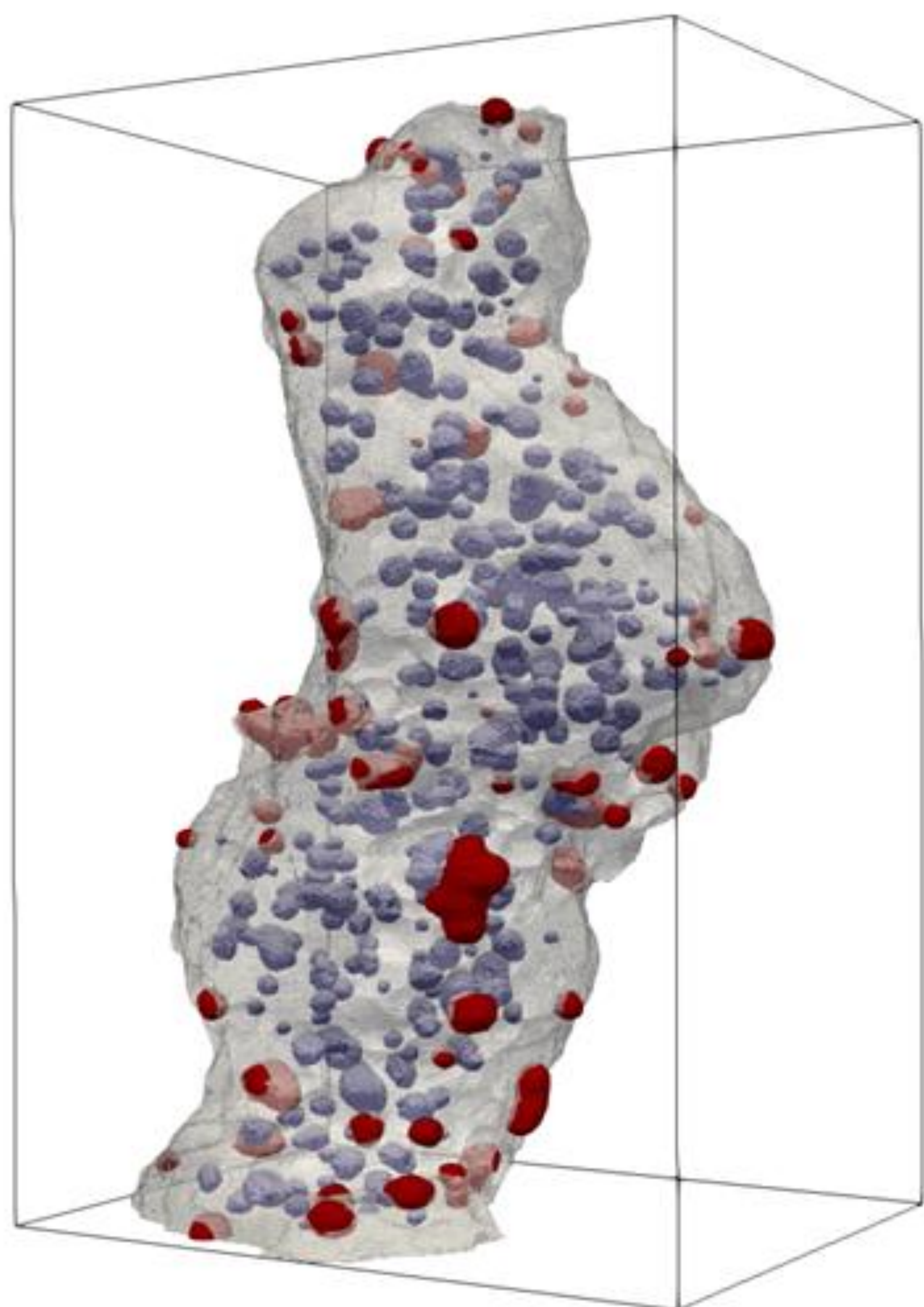


### Customized and final improved MEA

Different types of customised MEAs were investigated in FURTHER-FC. The influence of the type of carbon support, the Pt loading, the type and amount of ionomer (I/C Ionomer to carbon weight ratio) and the fraction of Pt on the carbon support were investigated. In addition to the reference, a total of 16 MEAs were planned to be prepared and **characterised**. Finally, based on our progress in understanding, the work was focused on 10 MEAs, with 9 customized and one final improved MEA, made with HOPI ionomer from The CHEMOURS Company.

Type of study	Catalyst	Pt Loading [ $\mu\text{g}/\text{cm}^2$ ]	I/C	Ionomer	Status
Effect of <b>type of support</b>	TKK HSAC 50%	200	0,8	D2020	Black
Effect of <b>Pt loading</b> (x3) (changing thickness)	TKK HSAC 50%	100	0,8	D2020	Green
	TKK HSAC 50%	500	0,8	D2020	Green
Effect of <b>thickness</b> by changing the Pt/C ratio Checked on two Pt loading and on two types of support	TKK Graphitized 50%	100	0,8	D2020	Green
	TKK HSAC 30%				Orange
	TKK Graphitized 30%	200	0,8	D2020	Green
	TKK Graphitized 50%				Orange
Effect of <b>I/C Ratio</b> (x2) Checked on two type of supports	TKK HSAC 50%	200	0,5	D2020	Green
	TKK Graphitized 30%				Orange
	TKK HSAC 50%	200	1,1	D2020	Green
	TKK Graphitized 30%				Orange
Effect of type of <b>ionomer</b> (x2) Checked on two types of support, two thicknesses by changing Pt/C ratio and two I/C	TKK HSAC 50%	200	0,5	HOPI	Green
	TKK HSAC 50%				Red
	TKK Graphitized 30%	200	0,8	HOPI	Green
	TKK HSAC 50%				Green
	TKK Graphitized 30%	200	1,1	HOPI	Orange

### Structure – Pt size distribution



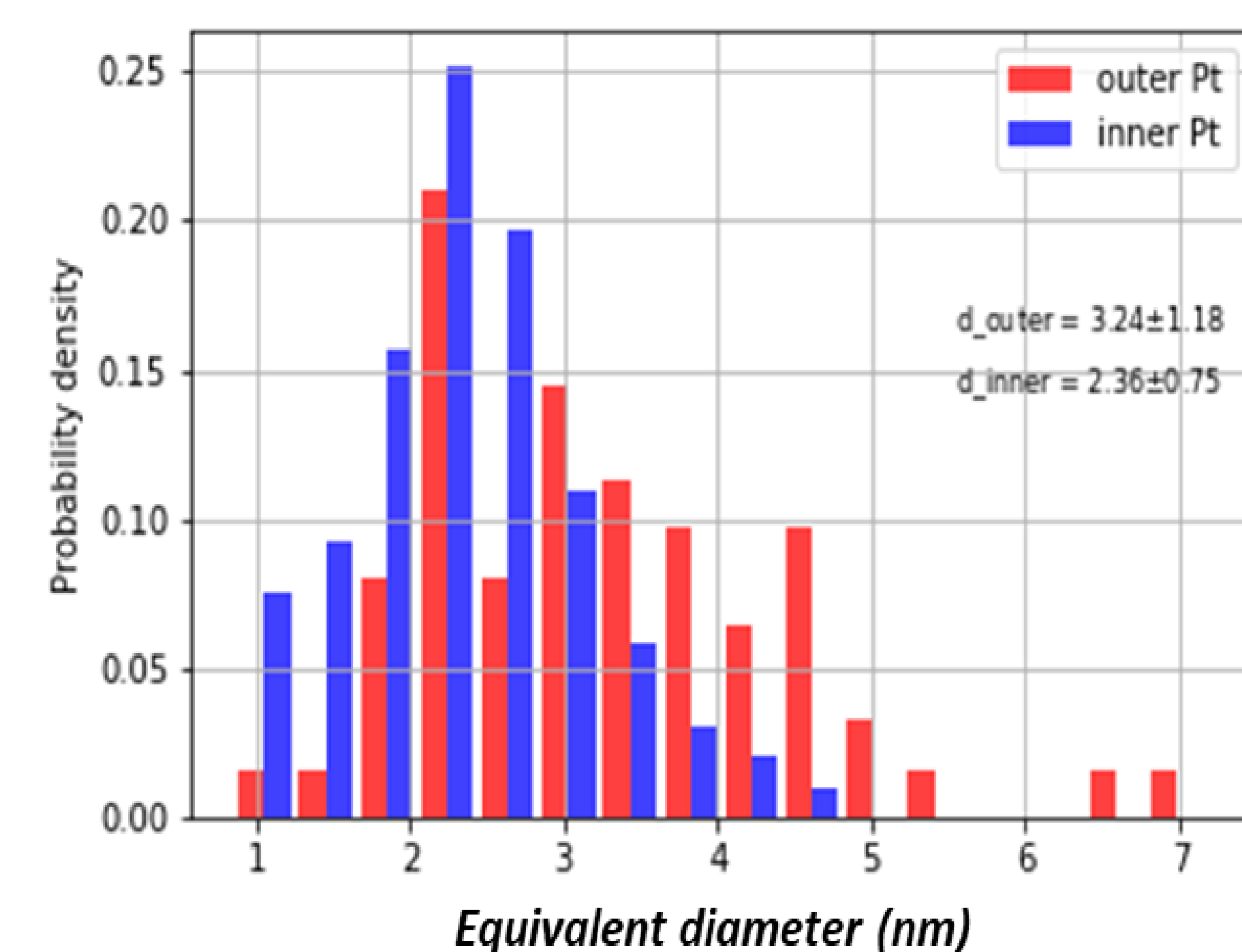
Outer Pt  
Inner Pt  
Carbon

The catalyst powder (TEC10E50E 46.2% Pt on high surface area carbon (HSAC) from Tanaka) was characterized by transmission electron microscopy (TEM). Since the HSAC support is nano-porous, some Pt nanoparticles are located in the carbon nano-porosity (inner Pt nanoparticles) and others are located on the surface of the carbon particles (outer Pt nanoparticles).

The diameter size of the outer (62 nanoparticles) and inner (294 nanoparticles) Pt nanoparticles were extracted from this 3D image and presented in .

The average nanoparticle diameters calculated from these histograms show that the outer Pt nanoparticles, with an average diameter of 3.2 nm, are slightly larger than the inner nanoparticles, with an average diameter of 2.4 nm. Calculation of the surface area of the Pt nanoparticles shows that 70% of the Pt surface area comes from the inner nanoparticles and 30% from the outer nanoparticles

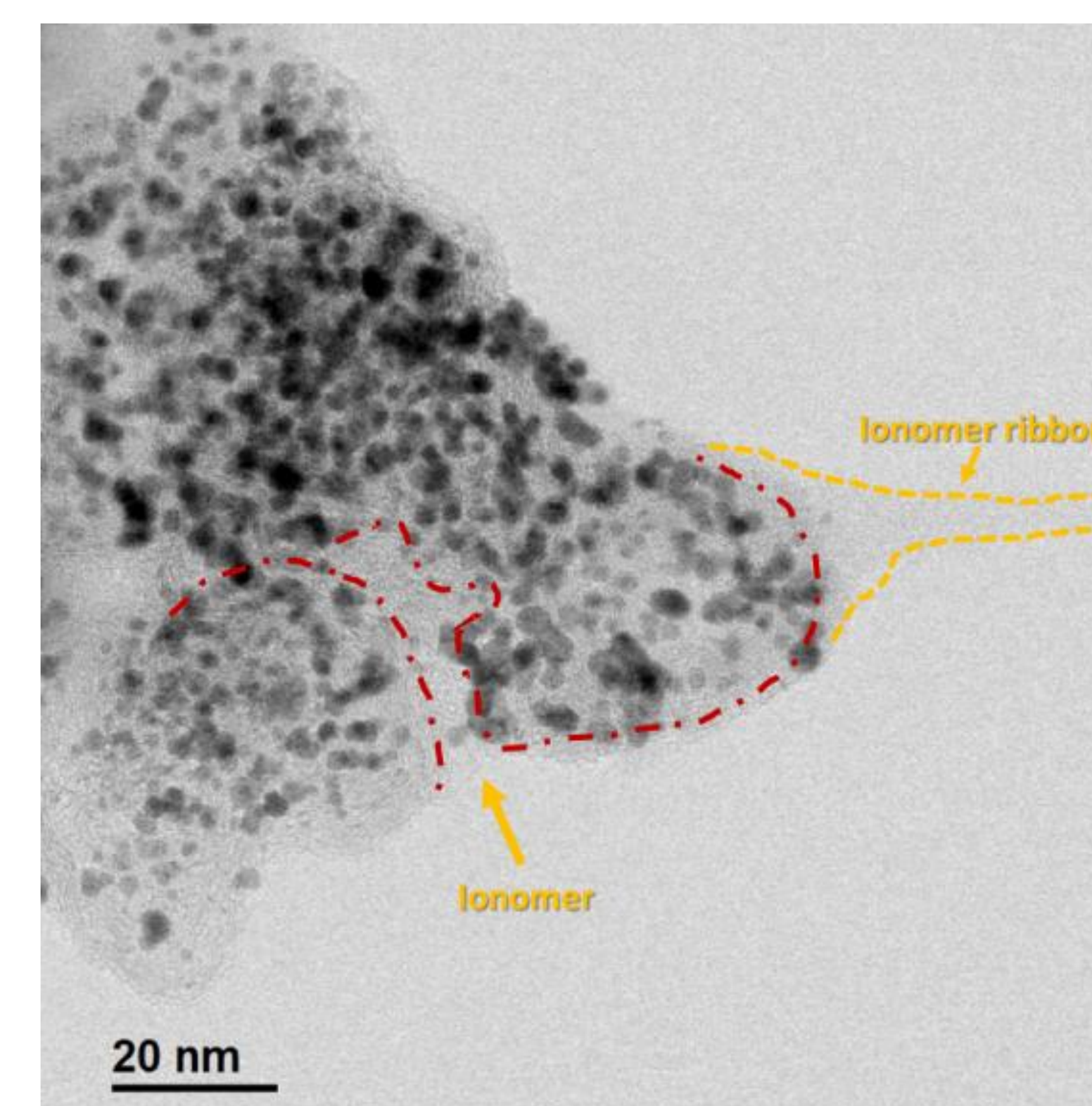
356 Pt NPs = 294 Inner Pt NPs + 62 Outer Pt NPs



### Structure Ionomer visualization

As a binder, and ensuring proton transport, the ionomer plays a crucial role in the CL. Its distribution and morphology will significantly affect the transport of proton both at the nanometer scale and through the thickness of the CL, and thus the Pt utilisation. So, considerable amount of effort is put into the characterisation and simulation of the ionomer morphology and distribution.

The distribution of the ionomer in the cathode was analyzed by TEM. For these analyses, a TEM sample preparation technique was developed by cutting thin slices of the MEA by cryo-ultramicrotomy without epoxy resin embedding.



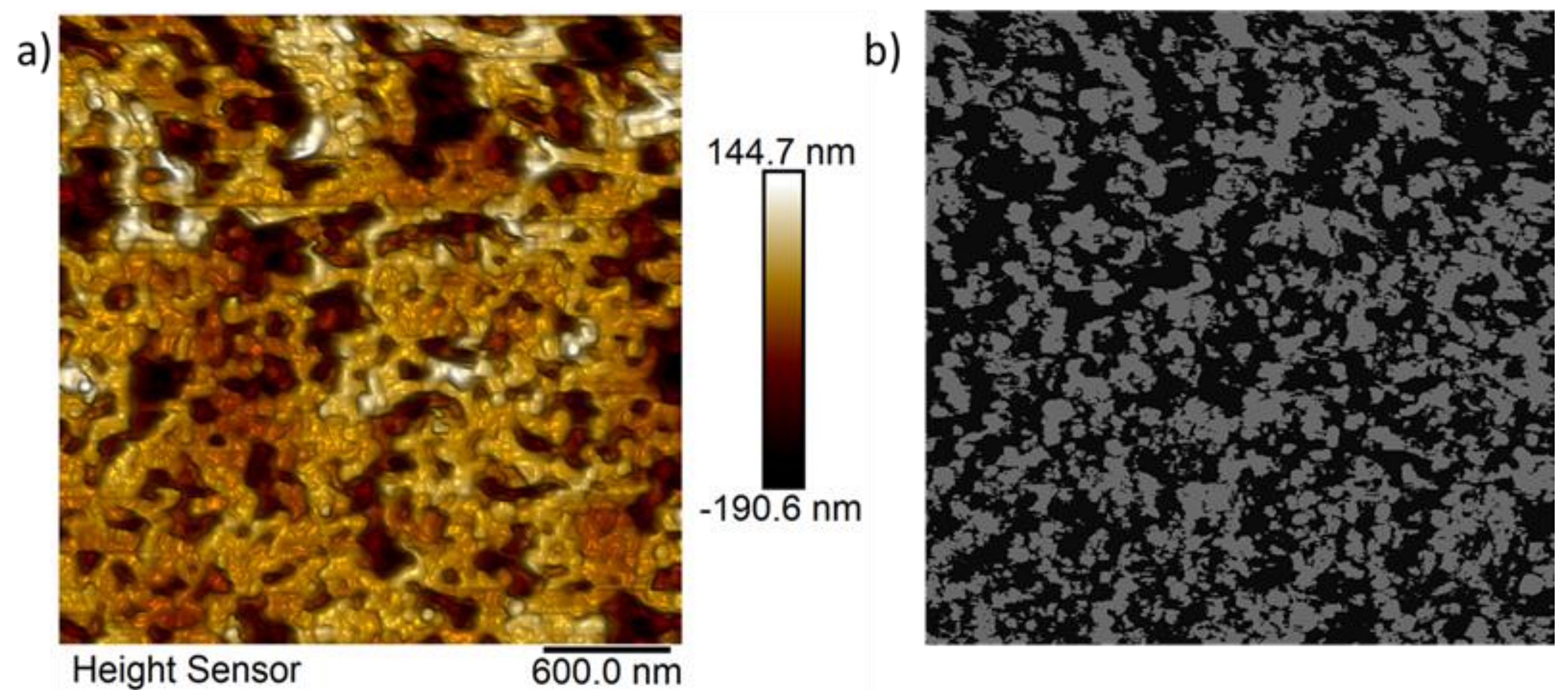
# FURTHER-FC Newsletter #6

## Further Understanding Related to Transport limitations at High current density towards future ElectRodes for Fuel Cells

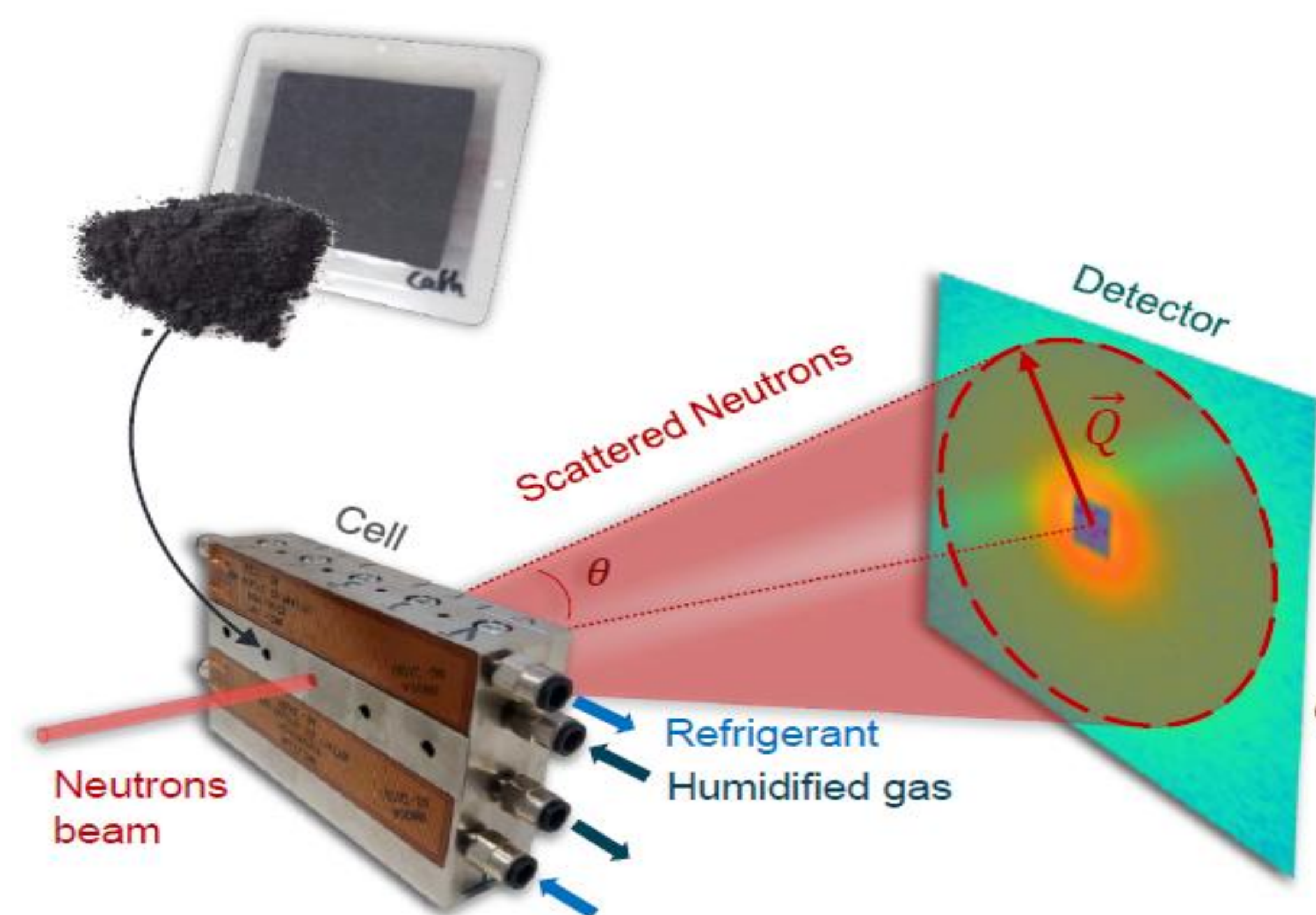


### Structure Ionomer visualization

With AFM the ionomer distribution can be measured using nanomechanical and nonelectrical properties. The differences of the ionomer in comparison to the catalyst particle are mainly seen in higher adhesion, higher deformation and also no electronic conductivity. An example of the Further-FC reference is shown in the Figure on the right. **Part a)** shows the measured height of the CCL surface while **part b)** is a representation of the ionomer distribution over the whole image based on the electronically isolating properties of the ionomer. The ionomer is shown in black in Figure b. In FURTHER-FC the ionomer coverage was compared for different ionomer to carbon ratios, different loadings as well as different carbon supports.



### Distribution/Structure of ionomer and water

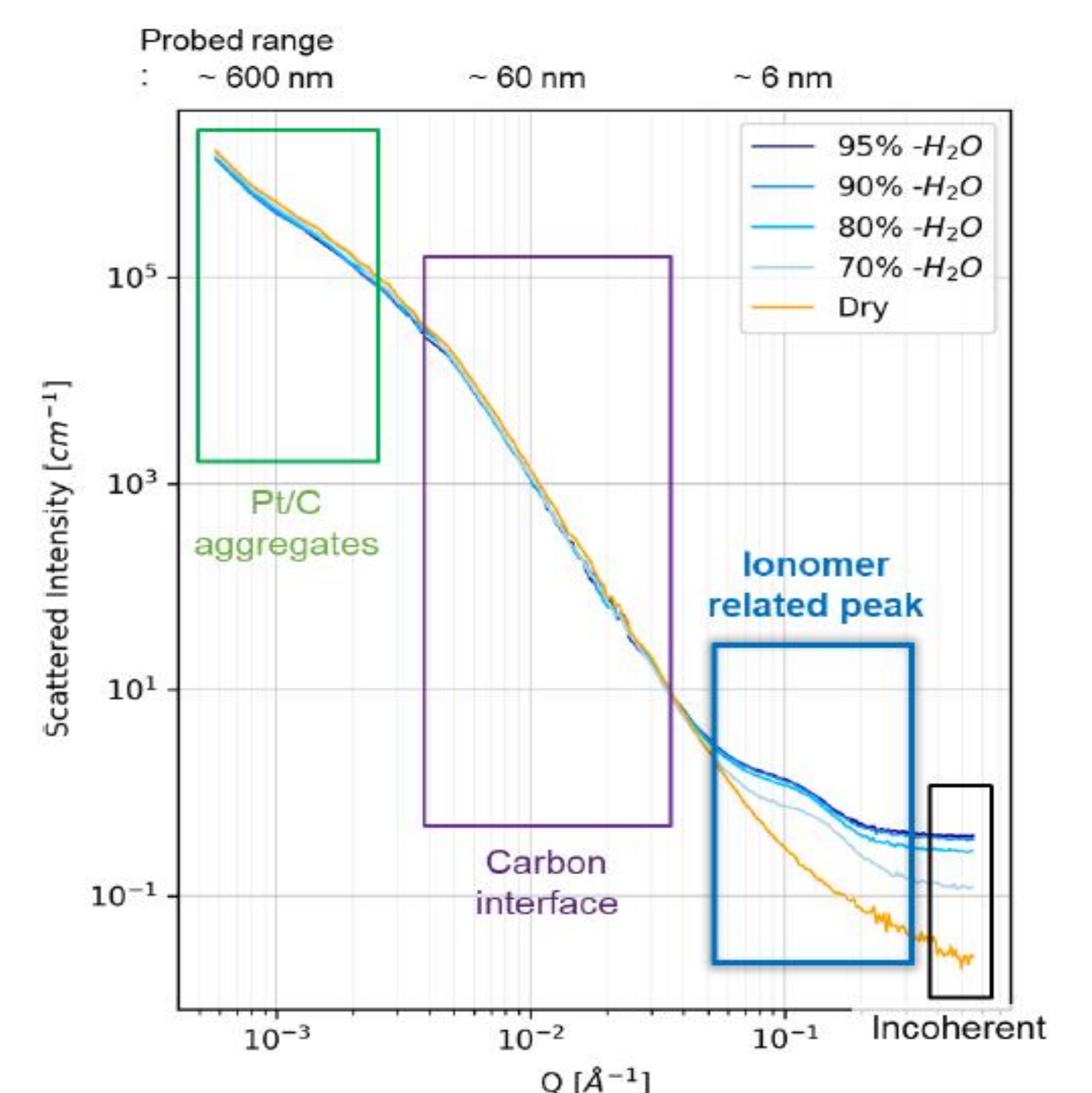


Small Angle Neutron Scattering (SANS) is a powerful tool to study the nanostructure of materials especially containing light elements, such as polymer and water. In FURTHER-FC we develop a methodology in order to quantify the structure of the catalyst layer, and especially we aim at quantifying the water content within the catalyst layer, its distribution (small or large pores) and the thickness of the ionomer film as a function of RH. These are crucial information in order to describe the transport phenomena in the CCL, and thus the CCL operation. This information averaged over the whole volume of the CCL is used into models developed in the project and results are compared to the characterizations done by AFM and electron microscopy that give a local information.

Two series of ex-situ measurements by SANS were performed in September 2020 and February 2021 by CEA on the D22 beamline of ILL as a function of RH on the reference CCL that was scratched from the reference MEA. The data have been analysed with models of structure and the results were published. To summarize, a 20 to 30 Å thick ionomer shell coats the Pt/C catalyst made from a Vulcan or high-surface area carbon (HSAC) support. For both catalysts, condensed water appeared at the ionomer/catalyst interface, even under 100% relative humidity. However, there are differences between smooth spherical particles from Vulcan and the rough and porous spherical particles from HSAC.

In the case of the HSAC support, the volume of condensed water at the carbon/ionomer interface is larger than that for the Vulcan carbon support because water fills the HAS carbon mesopores due to capillary condensation.

SAXS measurements at room temperature as a function of relative humidity have been performed on both reference and customised CCL made of 30 wt% Pt/GC by CEA at the ESRF (Figure on the top left). The evolution of the ratio of wet to dry profiles shows that capillary condensation of water in the smallest nanopores (3 - 8 nm) occurs first in the reference catalyst layer made of 50 wt%/HSAC. These pores are most likely located within the carbon primary particles containing Pt nanoparticles. The larger pores up to 20-30 nm are progressively filled. These pores most likely correspond to voids between the carbon primary particles. In the customised CCL made with 30 wt% Pt/GC, there is no evidence of these smallest pores accessible to water, as confirmed by TEM analyses and He pycnometry density measurements. Only the pores between the carbon primary particles are present. Further analysis would be required to determine saturation as a function of RH. However, it can be concluded from the larger decay of the intensity ratio for the reference CCL that there is much more water in the reference CCL than in the customised CCL made with 30 wt%Pt/GC.



# FURTHER-FC Newsletter #6

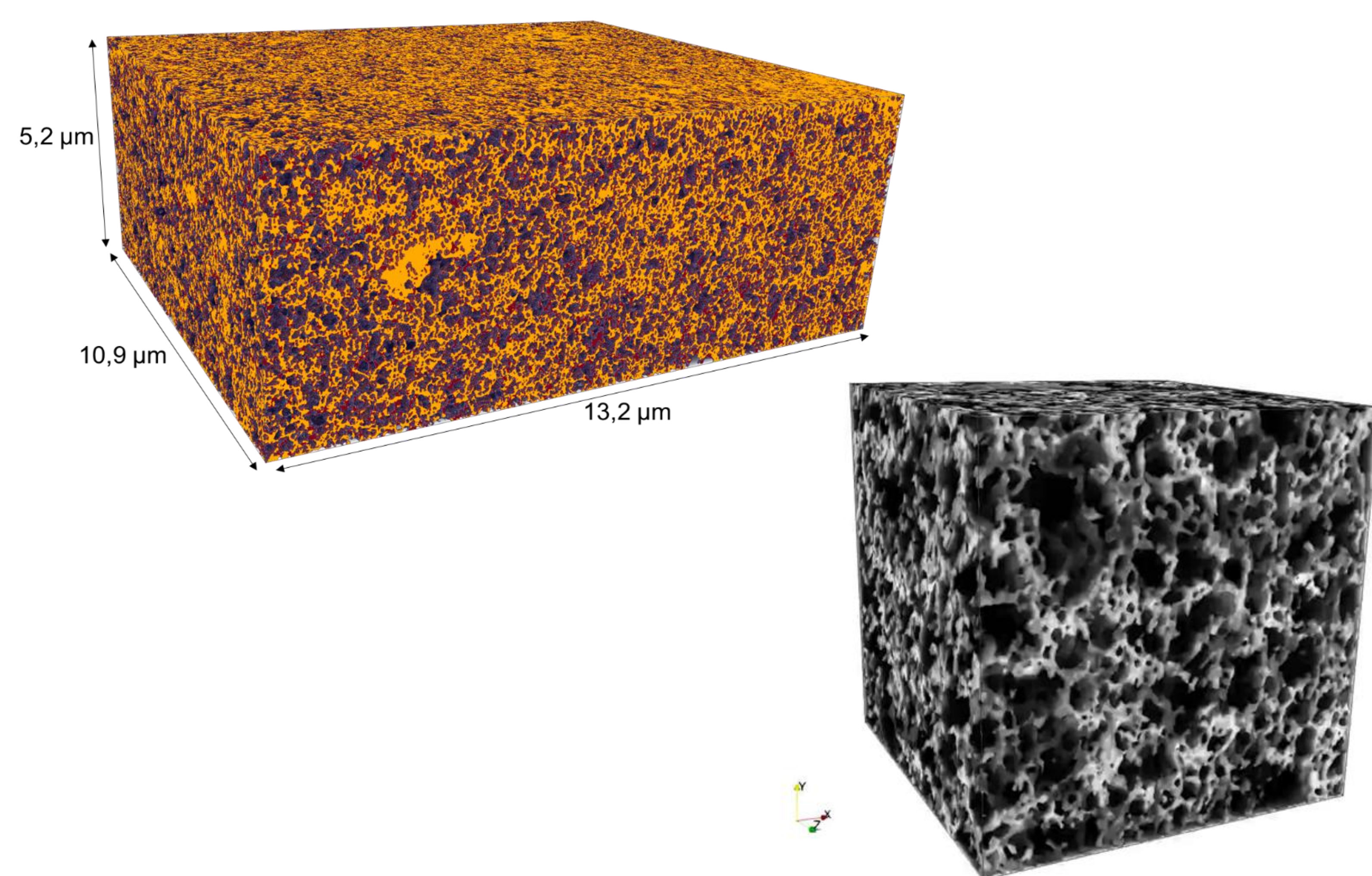
## Further Understanding Related to Transport limitations at High current density towards future ElectRodes for Fuel Cells



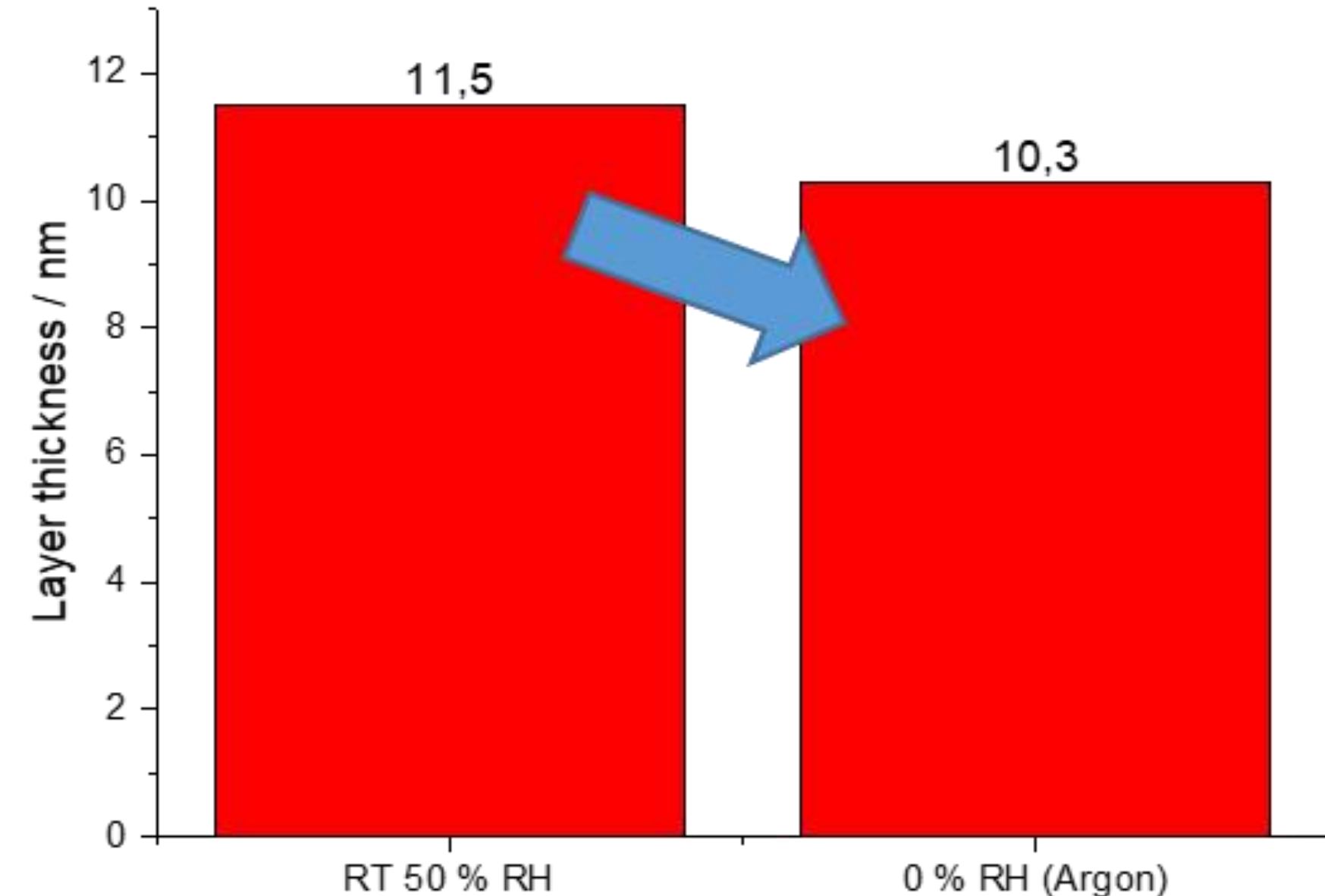
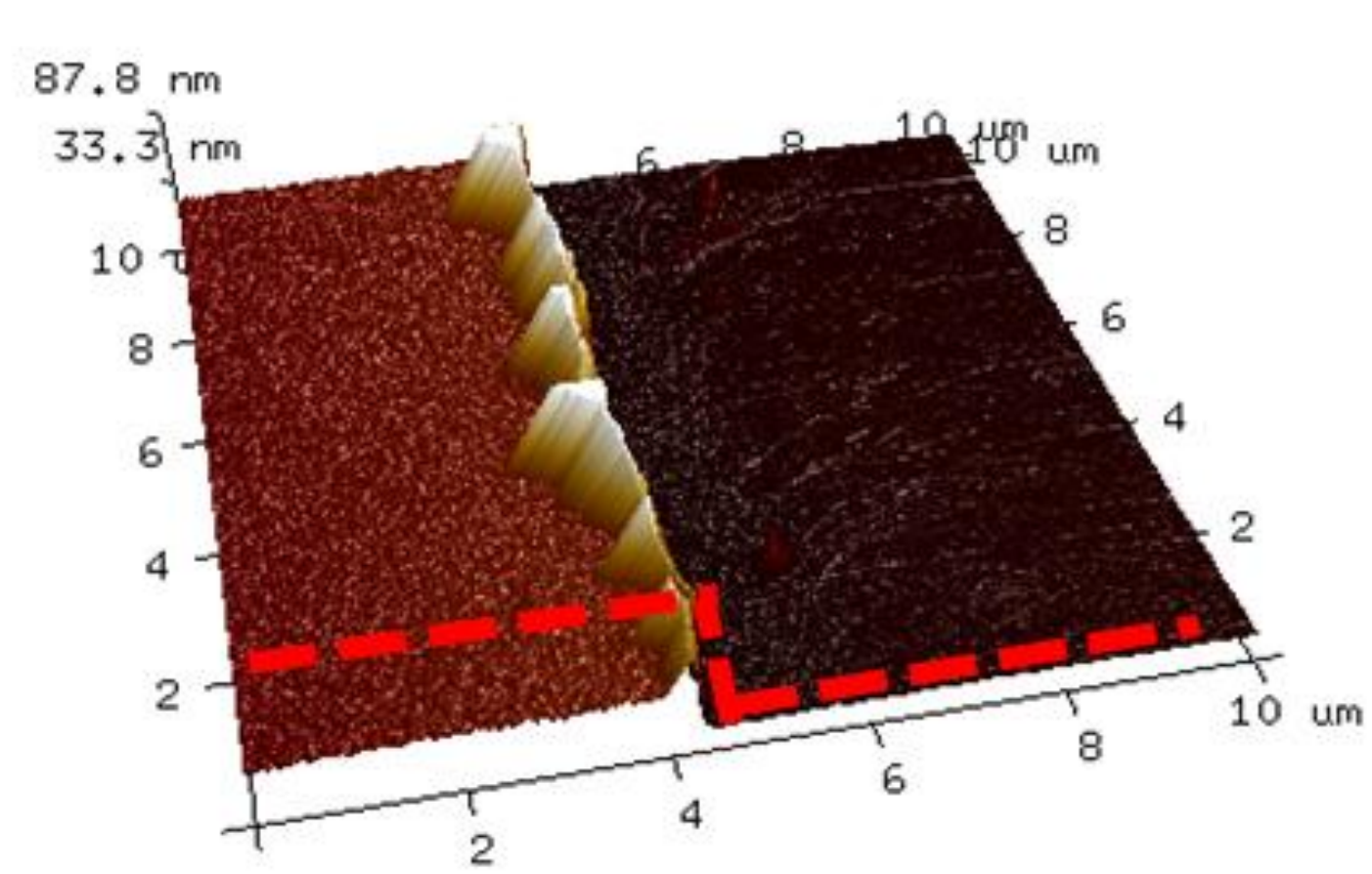
### Porous structure

The structure of the pore network determines the gas and liquid transport properties of the CL. Knowing the structure, it is possible to compute the local and effective transport properties of the CL.

The porosity of the FURTHER reference cathode was analysed by 3D FIB-SEM. The experiment was performed on the cathode without epoxy embedding with a voxel size of  $5 \times 5 \times 5 \text{ nm}^3$ . Figure 14a on the top left shows a 3D representation of a portion of the acquired SEM image stack where the carbon phase and porosity are clearly visible. Figure on the bottom left shows the 3D image with a size of  $13.2 \mu\text{m} \times 10.9 \mu\text{m} \times 5.2 \mu\text{m}$  after segmentation (porosity is in black). A porosity of 55% was calculated from this 3D image that is in agreement with the theoretical porosity calculated from the ink composition, Pt loading and cathode thickness.

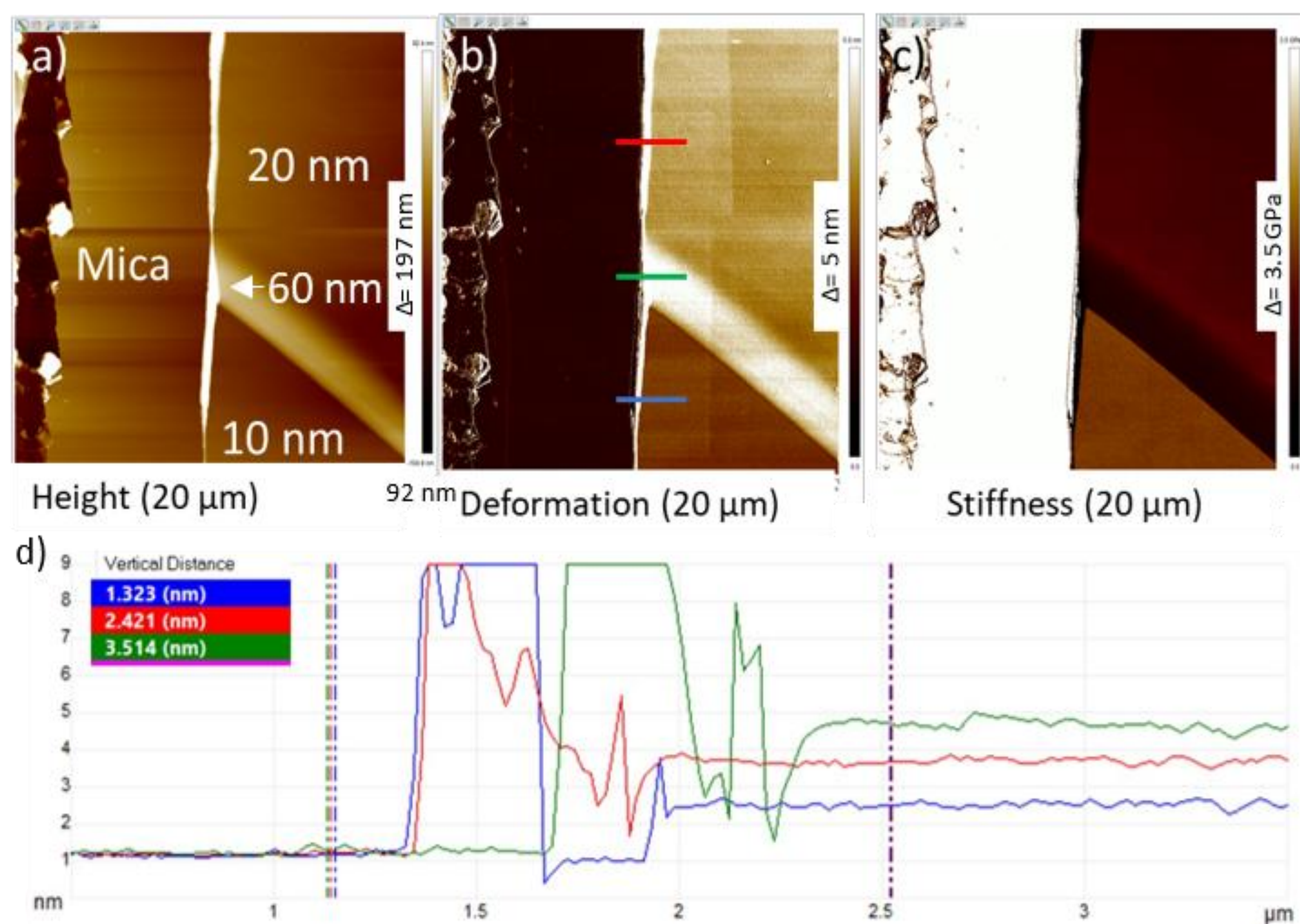
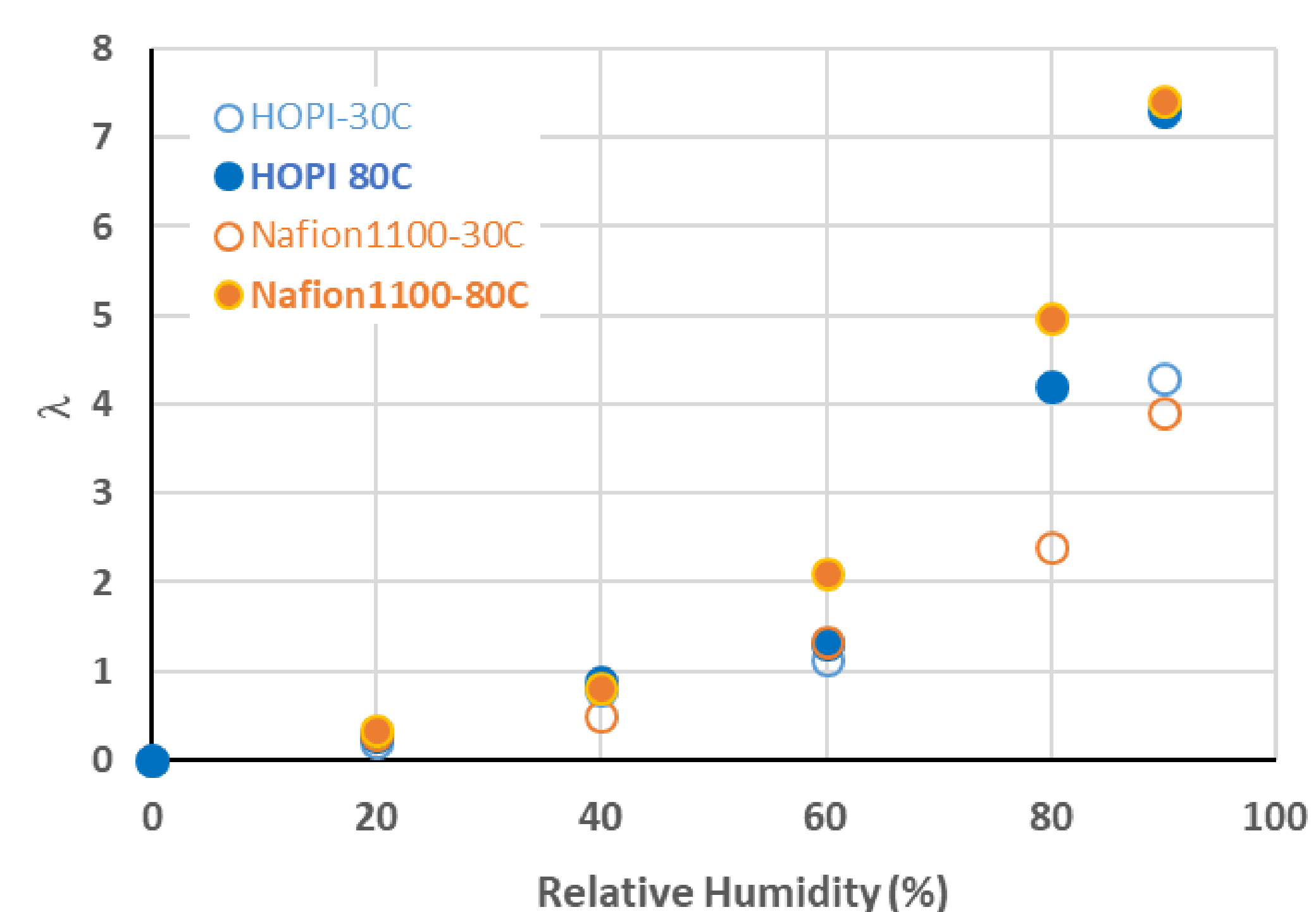


### Thin ionomer film properties



Nafion thin ionomer layers on different substrates and different thickness were produced and analyzed with AFM. The thickness of ionomer layers can be measured precisely and local with AFM. The ionomer layer is scraped off with AFM in contact mode by applying a high force and turning off the feedback electronics. When measuring perpendicular to the scratch the height difference can be evaluated like shown in Figure on the left. A decrease of the Nafion thin film thickness from 11.5 nm to 10.3 nm was measured for a RH difference from 50 % to 0 % (in argon atmosphere).

UCA used Quartz Crystal Microbalance (QCM) to determine the average number of water molecule per sulfonic acid group ( $\lambda$ ) as a function of relative humidity at 30 and 80°C within 10 nm thin Nafion 1100 g/mol and HOPI films



Nanomechanical properties are expected to change with different ionomer thickness. The local measurement of nanomechanical properties can provide a direct correlation between thickness and properties (on the left). The change in nanomechanics was measured for an ultra-thin ionomer (Nafion) layered structure on mica with varying ionomer thickness. A data set for a square of  $20 \mu\text{m}$  side length is shown in Figure 17: The measurement of the height is shown in Figure. Three areas of different thickness are visible in the measurement: 10 nm, 20 nm and 60 nm with a clear contrast in the deformation and stiffness measurement. Deformation when applying a given force (in the middle) increases as the ionomer layer thickness increases. Stiffness is highest for lowest ionomer thickness (on the right). The lower part shows the deformation data measured along the marked lines in the upper data set with the difference to the substrate indicated in the upper left corner. Also, the difference to the substrate (left side, mica) is visible. The aim of this study is to compare the values to real catalyst layers to directly estimate the thickness of the ionomer layer. For this purpose, different substrates were analysed with their influence on the resulting stiffness.

From measurements of non-covering ionomer layers, making the ionomer bundles visible, it was found that the deformation is higher for the isolated single bundles not embedded in a matrix of other ionomer bundles.

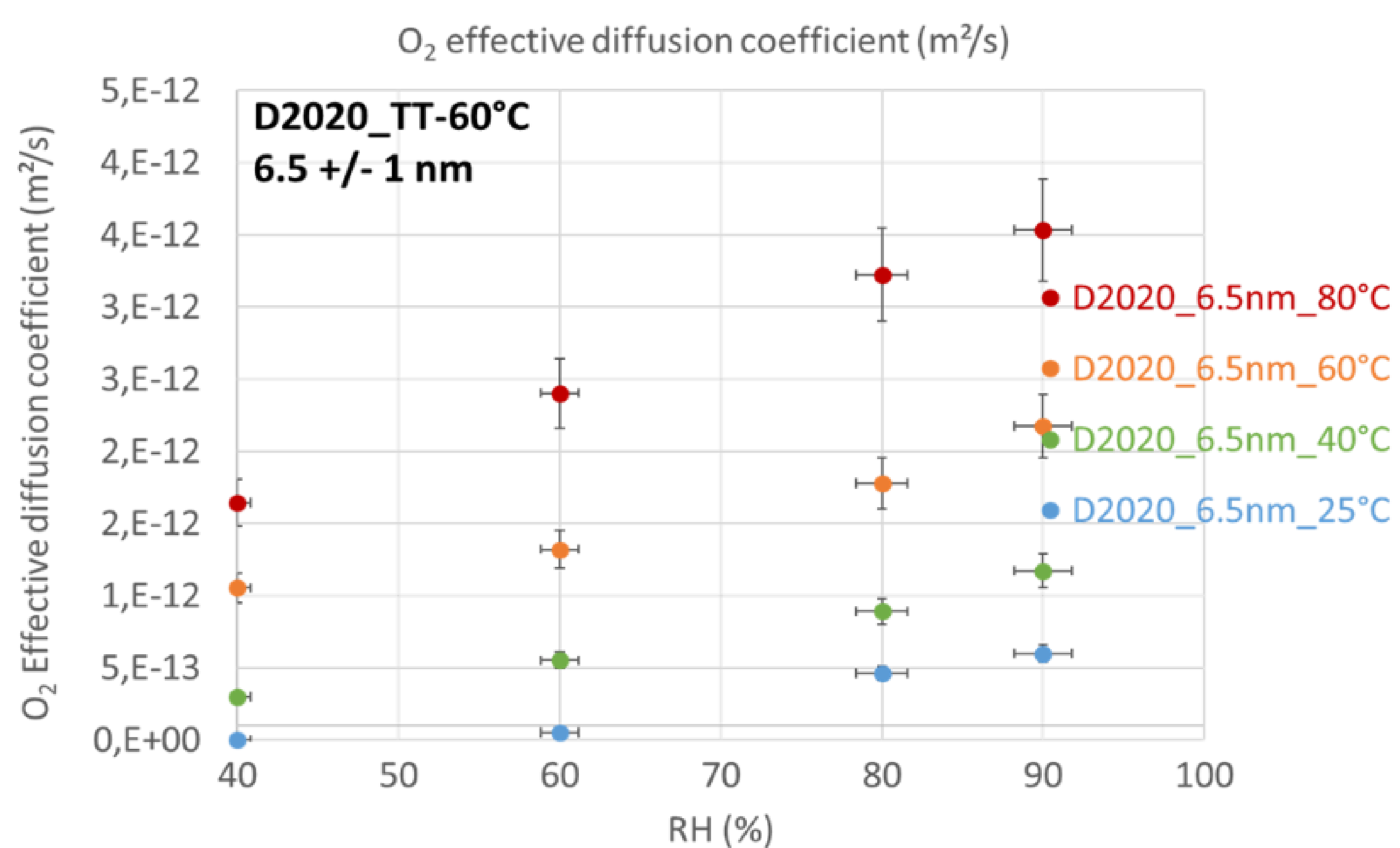
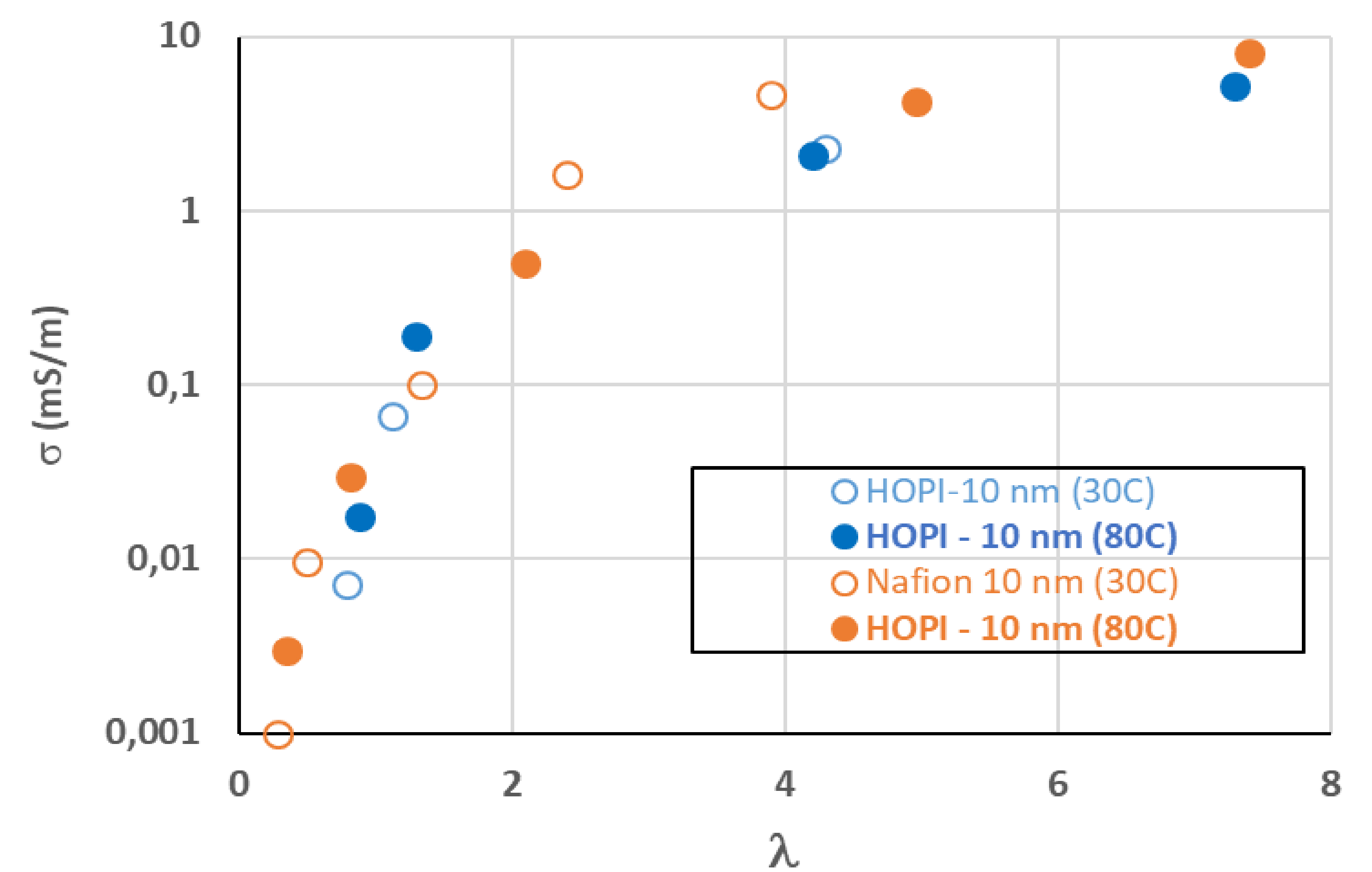
# FURTHER-FC Newsletter #6

## Further Understanding Related to Transport limitations at High current density towards future ElectRodes for Fuel Cells



### Thin ionomer film properties

The proton conductivity of ionomer films with thickness down to 10 nm have has-been calculated by UCA and CEA as a function of relative humidity based on impedance measurements using interdigitated array microelectrodes (Figure to the right). As expected, the conductivity increases with RH for a given temperature. The conductivity is much smaller than the conductivity measured on bulk ionomer membrane, as expected from previously published results. The results obtained at CEA and UCA are in good agreement. The conductivity of the HOPI supplied by CHEMOURS is similar to that of Nafion with an EW of either 1000 or 1100 g/mol. The conductivity increases with temperature for a given RH. It is possible to plot these values as a function of water content in average number of water molecule per sulfonic acid group instead of RH, using the values of water uptake as a function of RH determined from through-plane swelling of the film calculated from QCM measurements by UCA (Figure below). The water content ~~that~~ which is increasing ~~increases~~ with temperature for a given RH seems to ~~rule~~ dominate the conductivity, rather than just the RH itself. Indeed, all films show the same conductivity for a given water content, whatever the chemistry and temperature.



In the frame of FURTHER-FC, CEA has developed a method to calculate the bulk and interfacial effective  $O_2$  transport resistance of ionomer thin films having thickness values down to 10 nm, based on  $O_2$  limiting current analysis (LCA). The concept is similar to that reported by Kudo et al. The limiting current under  $O_2$  has been measured for films of different thickness. From these measurements, with simplification hypotheses, it is possible to calculate effective  $O_2$  diffusion coefficient (Figure 20 on the left). CEA specifically designed and manufactured a dedicated setup to ease the measurements. The method has been patented and the results will be published. The values will be integrated into the models in order to compute the transport limitations in the CCL.

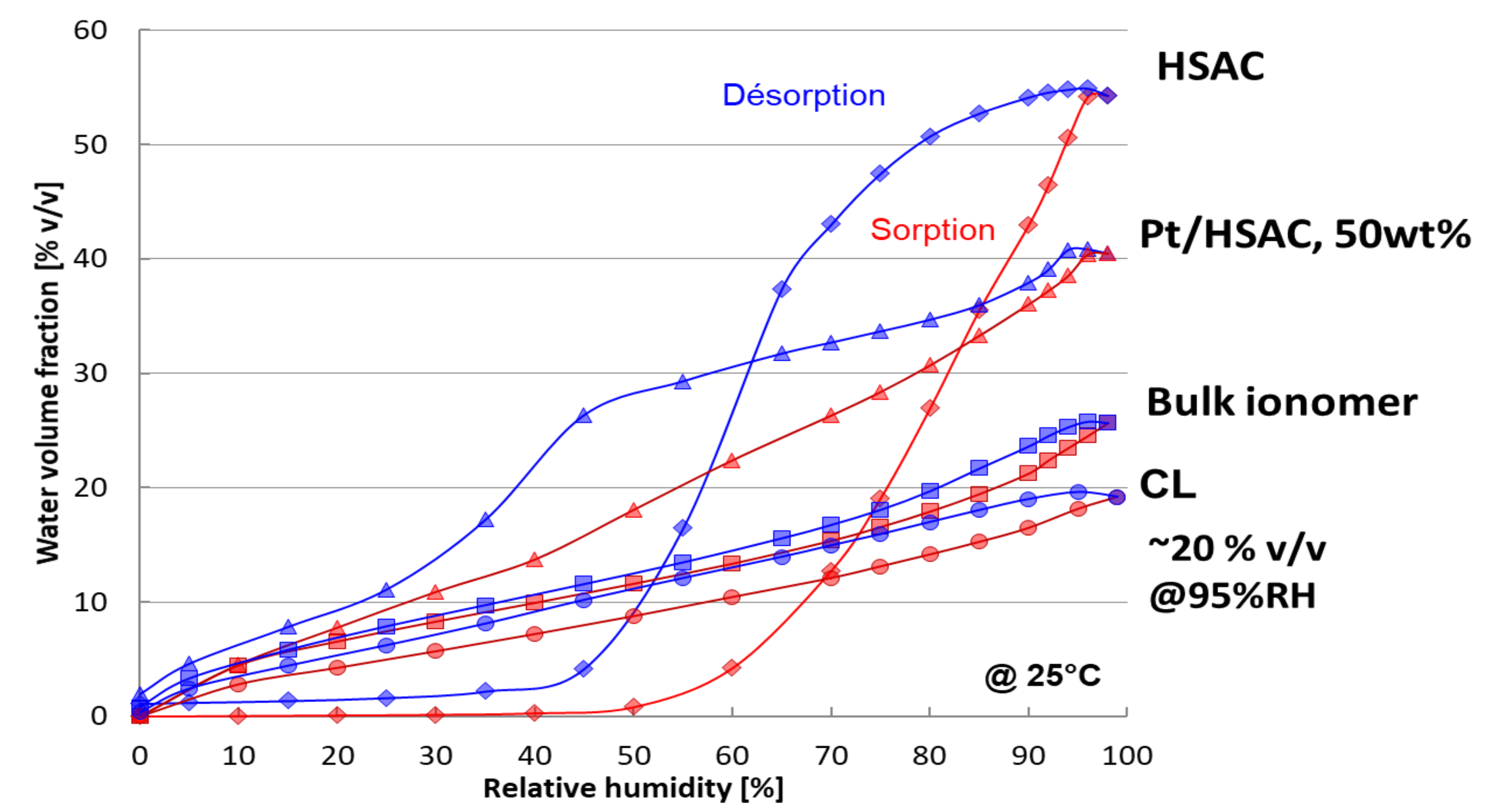
# FURTHER-FC Newsletter #6

## Further Understanding Related to Transport limitations at High current density towards future ElectRodes for Fuel Cells



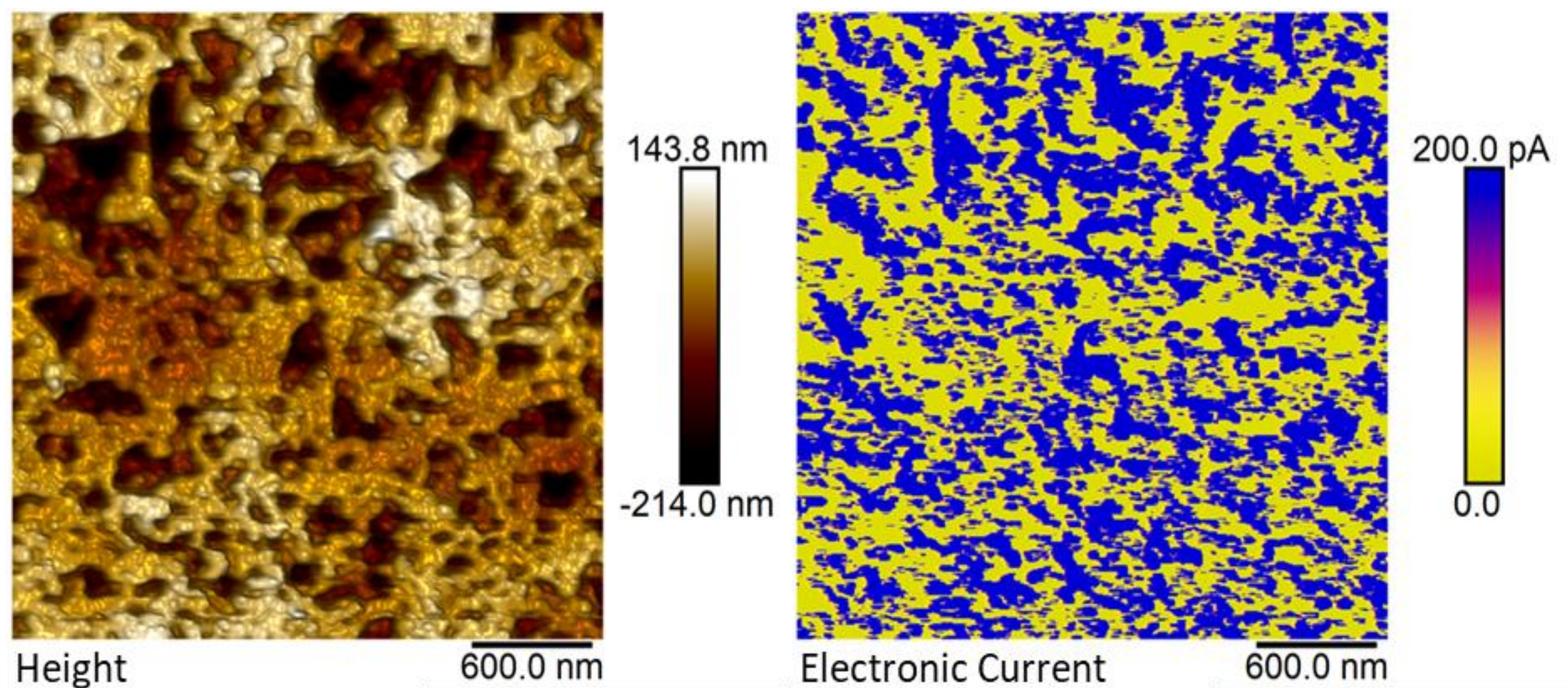
### CCL PROPERTIES

Water vapour sorption isotherms were measured on HSAC, 50 wt% Pt/HSAC, D2020 bulk ionomer and a catalyst layer of Pt/HSAC and D2020. It can be clearly seen that the carbon is very hydrophilic and swells a lot of water, indicating the presence of polar groups. The hysteresis between sorption and desorption is large, which is probably an indication of the nanoporous structure of the HSAC. More surprisingly, the catalyst layer contains less water by volume than the individual components, indicating that the ionomer in the catalyst layer most likely swells less than the bulk ionomer and that the ionomer most likely blocks some pore of the catalyst.



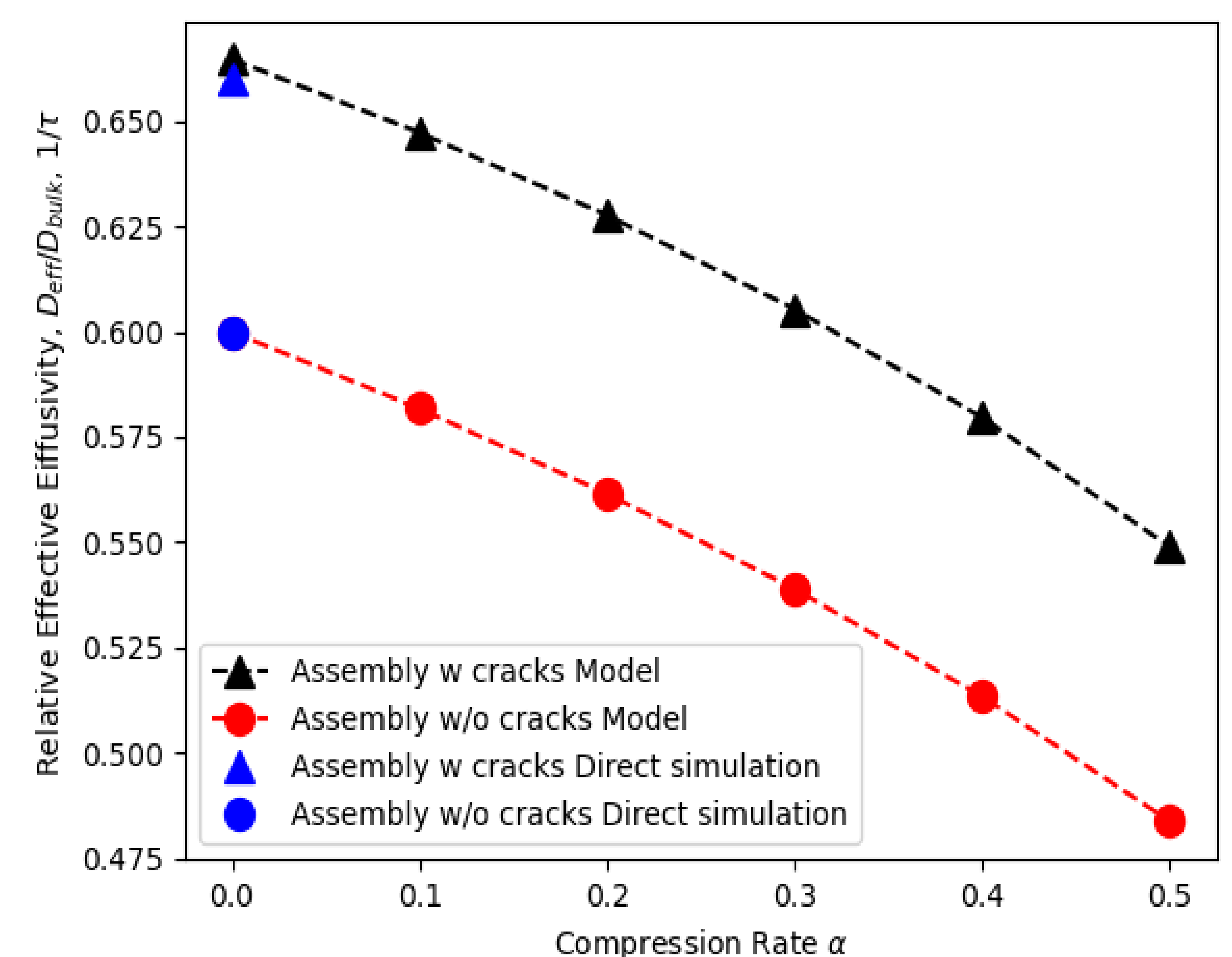
The effective transport properties in the CCL which can be measured with AFM are electronic and proton conductivity as well as thermal conductivity.

The electronic conductivity can be measured with any conductive AFM probe. For proton conductivity a catalytically active AFM tip is needed, as the reaction takes place at the AFM tip which acts as nanoelectrode. Exemplary result of the electronic conductivity of MEA on area of 3  $\mu\text{m}$  side length are shown here on the right.



### Computation of properties from 3D structure

Transport properties (diffusion tensor, thermal conductivity tensor, electrical conductivity tensor,...) or equilibrium properties (capillary pressure curve, etc) of PEMFC components (catalyst layers, GDL,..) are key input properties for simulation models developed for understanding better how a PEMFC operates or as tools to help improve performance via better design and study crucial issues such as the water management or the aging of PEMFC. Obtaining these properties from experiments is possible (as illustrated in Section 4) but often difficult, notably because these components are thin porous media (with thicknesses between a few tens of micrometers and a few hundreds of micrometers depending on the component). With the development of imagery techniques, an alternative is to compute these properties from numerical simulations on three dimensional digital images of the component microstructure.



### GDL

In FURTHER project, this approach was developed for the study of a GDL combining two imagery techniques. The first one is the FIB-SEM technique. This technique allows obtaining three-dimensional images of microstructures with pores in the nanometer range. The second one is the X-ray microtomography technique. This technique allows obtaining three-dimensional images of microstructures with pores in the micrometer range. Hence combining the two techniques allows studying components with a wide range of pore sizes.

# FURTHER-FC Newsletter #6

## Further Understanding Related to Transport limitations at High current density towards future Electrodes for Fuel Cells



### DNS and pore network modeling of MPL/GDL

DNS are performed on 3D digital images of component microstructures obtained by FIB-SEM (Focused Ion Beam Scanning Electron Microscopy, CCL) or a combination of FIB-SEM and X-ray tomography (gas diffusion layer, GDL).

This allows computing **macroscopic properties** such as,

- the effective diffusion tensor
- the thermal conductivity tensor
- the electrical conductivity tensor

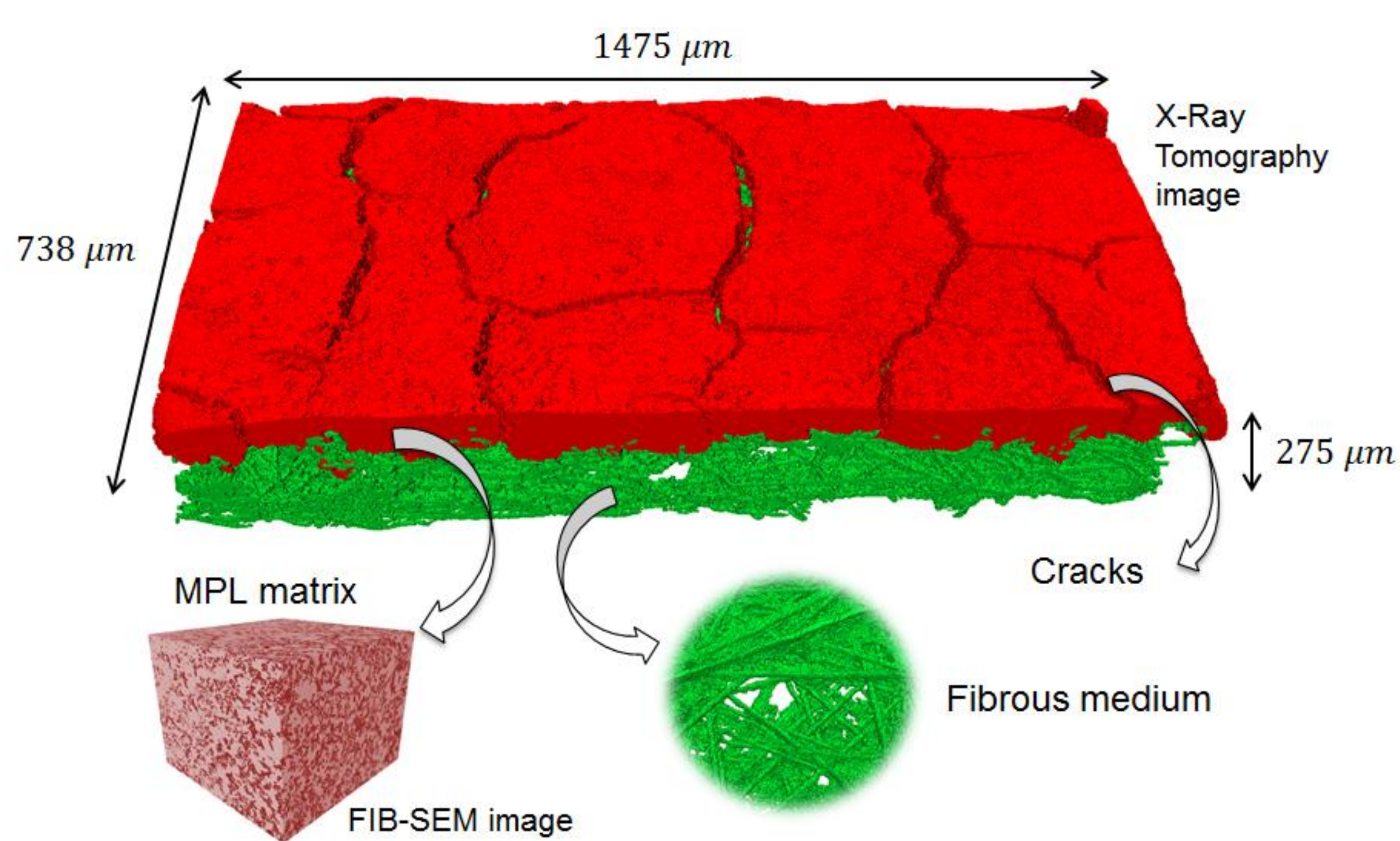


Figure 6. 3D digital image of GDL combining X-ray Tomography (fibrous medium, cracks) and FIB-SEM (MPL matrix)

- Simulations show the importance of Knudsen diffusion
- Impact of cracks in the MPL (MicroPorous Layer) on the oxygen diffusive transport through the GDL has been assessed.

**Pore size distributions** are determined by extracting the pore network from the 3D digital Images of microstructures using the open source softwares Porespy and OpenPNM

Results are in good agreement with experimental data obtained by Mercury intrusion porometry.

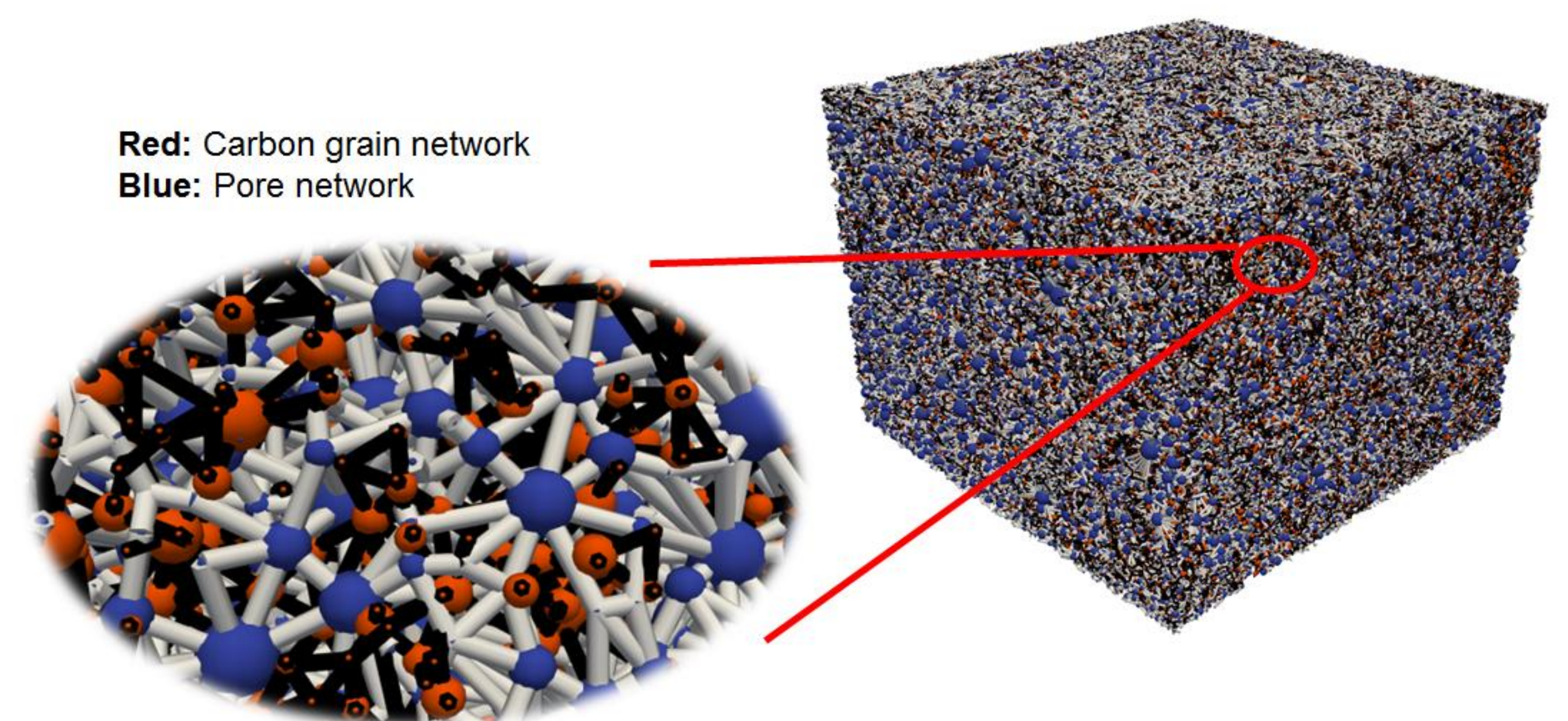


Figure 7. Pore and Carbon grain network extracted from a MPL matrix 3D FIB-SEM image using Porespy / OpenPNM

- Computations of effective properties on the extracted networks (solid phase network and pore network) are validated against DNS results.
- Network computations of effective properties are much faster than DNS

### Volume averaged multi-scale modeling of single cell

A 2D differential cell model has been implemented in the DLR modeling framework NEOPARD-X. The model includes formulations for

- Two-phase multicomponent transport
- Energy transport
- Charge transport
- Water sorption kinetics
- Transport through the ionomer film
- Gas crossover through the membrane
- Hydrogen Oxidation Reaction (HOR) and Oxygen Reduction Reaction (ORR) kinetics
- Platinum oxide formation

In the course of the project the initial sub-models will be revised and improved based on the outcomes obtained from the lower scale models.

An **in-depth model validation** with dedicated experiments performed in differential cells is on-going in order to identify the accuracy and limitations of the current model. These experiments include

- Polarization curves with various O<sub>2</sub> concentration in N<sub>2</sub> and He
- Impedances under H<sub>2</sub>/air and various oxygen concentrations
- Impedances under H<sub>2</sub>/N<sub>2</sub>
- Limiting current measurements in nitrogen and helium

First simulation results suggest the importance of the ionomer film resistance as well as of the cracks in the MPL for an accurate description of the cell performance.

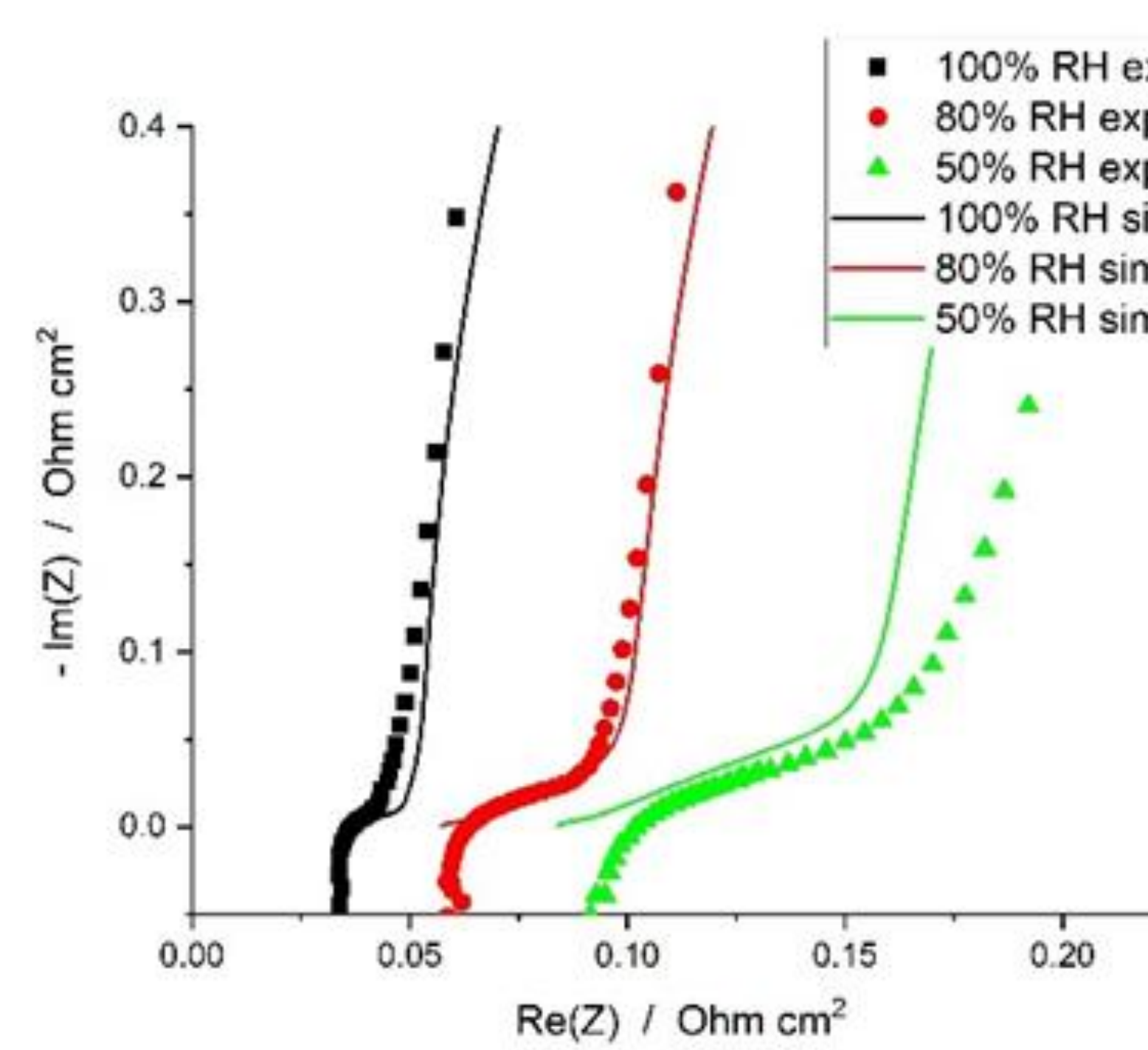


Figure 8. Validation with impedances under H<sub>2</sub>/N<sub>2</sub>

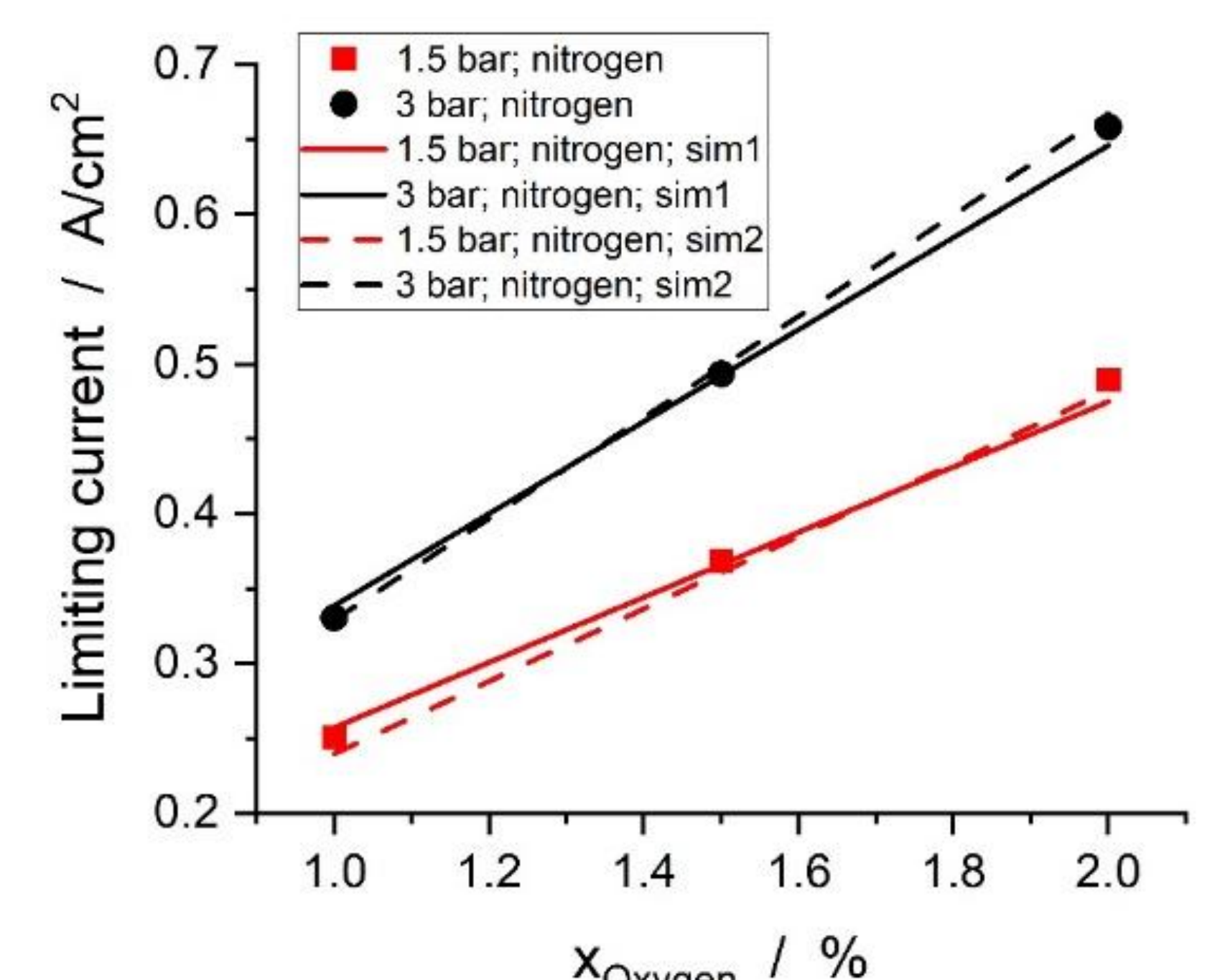
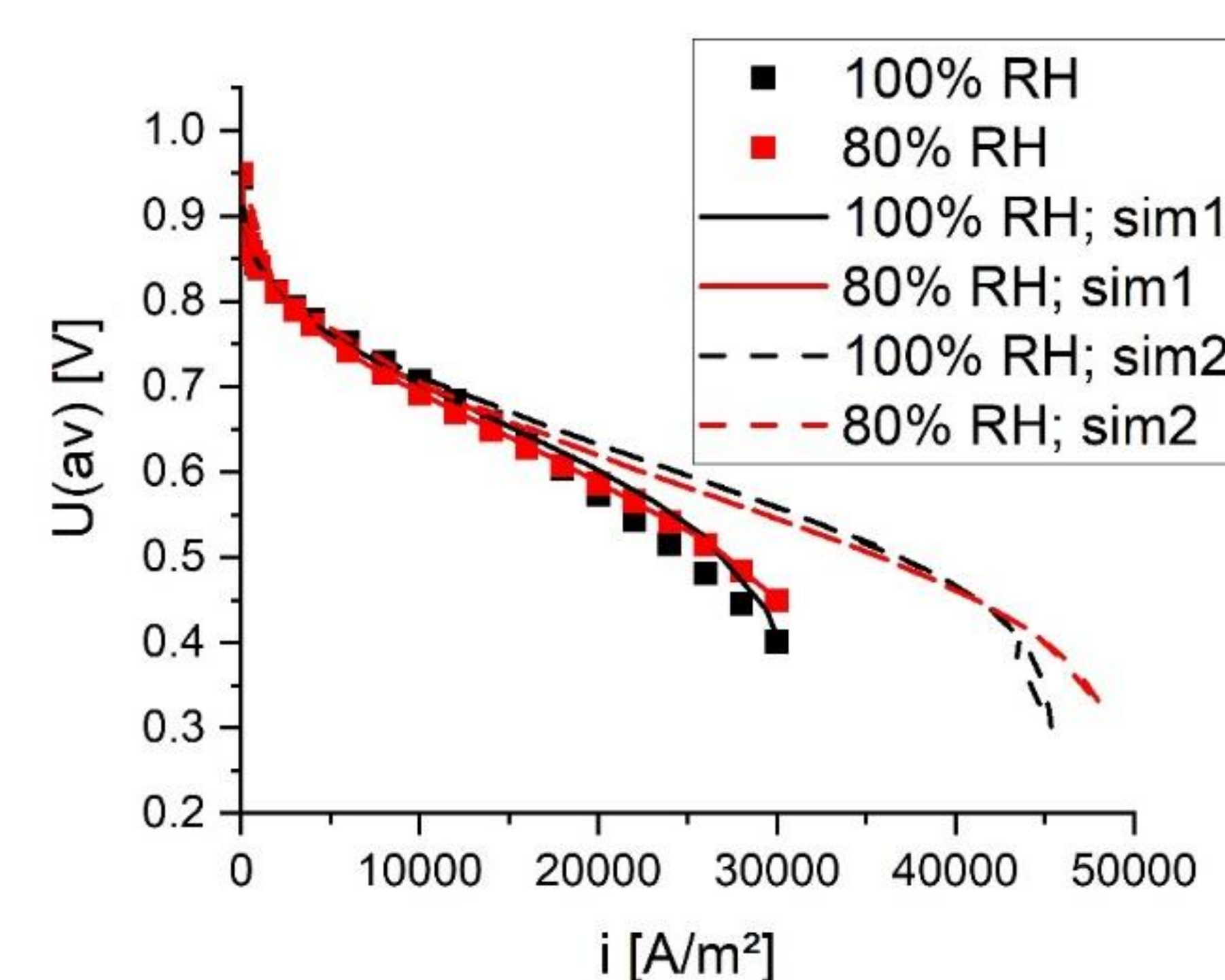


Figure 9. Validation with limiting current analysis



# FURTHER-FC Newsletter #6

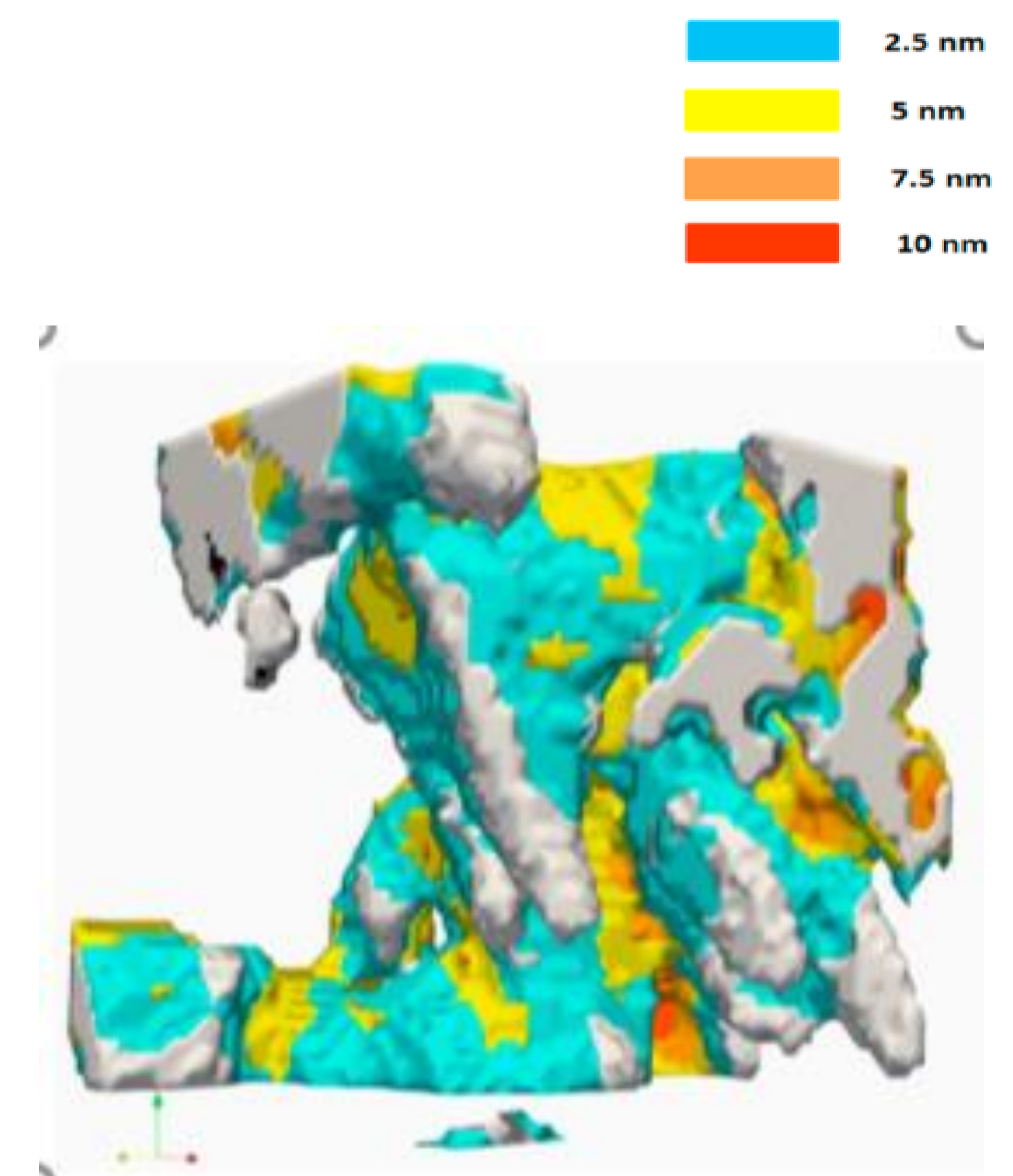
## Further Understanding Related to Transport limitations at High current density towards future ElectRodes for Fuel Cells



### Computation of properties from 3D structure

Numerical simulations were also developed to characterize CCL properties from the CCL 3D digital image obtained by FIB-SEM (Figure 28). The main results can be summarized as follows:

A computational method was presented for studying the ionomer distribution in the CCL and reconstructing the ionomer distribution in the three-dimensional image (on the right). The method is based on the consideration of three forms of ionomer structure: the ionomer distributed under the form of ionomer filaments partially occupying the secondary pore space, the ionomer thin films partially coating the wall of the secondary pores and the inter-carbon grain ionomer localized inside the FIB-SEM segmented solid phase. The method allows reconstructing the ionomer coating and the ionomer filaments over the full size of the CCL FIB-SEM image, i.e. over representative images of the CCL microstructure. The reconstructed coating ionomer is found to form a well-connected percolating network over the CCL thickness. The inter-carbon grain ionomer is considered as ionomer coating the Pt-carbon grains inside the FIB-SEM image segmented solid phase.



The CCL oxygen effective diffusion and effective proton conductivity full tensors were characterized. The results show that the obtained tensors are not isotropic. They confirm that Knudsen diffusion has a significant impact and must be considered together with Fick diffusion.

The results show that the effective proton conductivity is heterogeneous at the scale of the computational domains typically considered in many previous works due to the variability in the ionomer distribution at this scale.

Contrary to previous works based on numerical simulations on synthetic images, which tend to underestimate the proton effective conductivity through-plane component, our results are globally in better agreement with experimental data. This is considered to be due to the better representativity of the CCL microstructure obtained via the FIB-SEM imaging compared to synthetic images. This is also seen as an indicator of the relevance of the developed ionomer reconstruction procedure.

The simulations indicate that the transport in the inter-agglomerate ionomer has an impact in addition to the transport in the coating ionomer but not sufficiently for changing significantly the comparison with the experimental data.

The impact of liquid water in the primary pores on the proton transport in conjunction with the transport in the ionomer was also explored. The simulations indicate a significant impact, that could potentially reconcile the simulations and the experimental data.

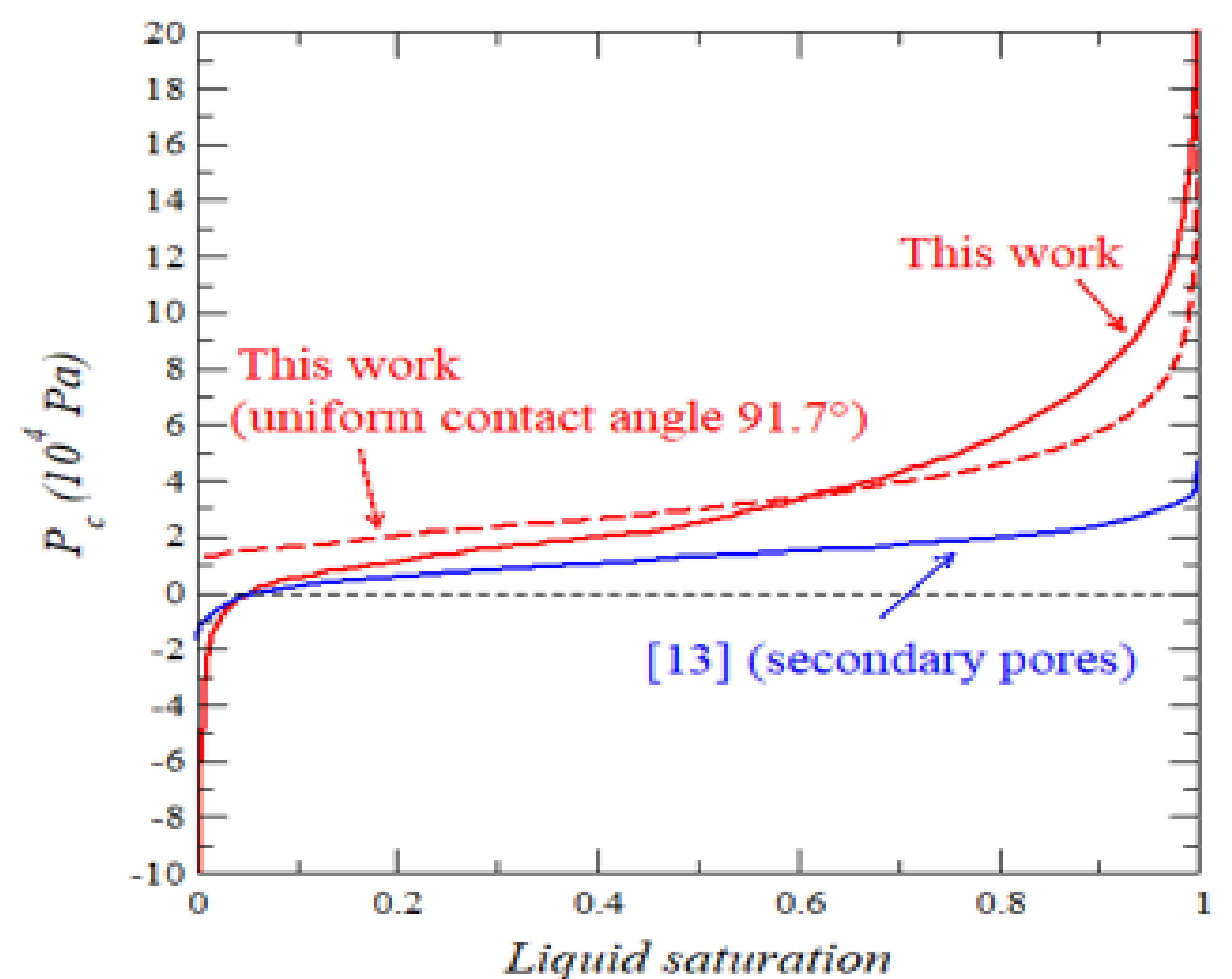
In spite of the encouraging results obtained via the combination of FIB-SEM imaging and the developed ionomer reconstruction procedure, all this shows that further work is still needed to better characterize the morphology of the ionomer in the CCL and the proton transport in the CCL.

The wettability properties of the CCL was characterized via a numerical approach enabling one to determine the contact angle distribution in the three dimensional digital images of the CCL microstructure obtained by FIB-SEM after reconstruction of the ionomer coating and ionomer filaments.

The results illustrate the key role of the ionomer on the wettability properties. The latter highly depend on the ionomer distribution within the CCL microstructure and in particular on the ionomer coating the secondary pore walls.

The concept of effective contact angle was also used at the pore scale after segmentation of the pore space into individual pores. This leads to associate an effective contact angle with each pore. The 3D images so obtained are well suited for simulations of two-phase flows and computations of the water retention curve and relative permeabilities from PNM simulations or image-based techniques such as the full morphology approach.

The results give insights into the correlation between the pore size and effective contact angle. The combined information on the pore size and the effective contact angle for each pore was used to obtain the water retention curve.



# FURTHER-FC Newsletter #6

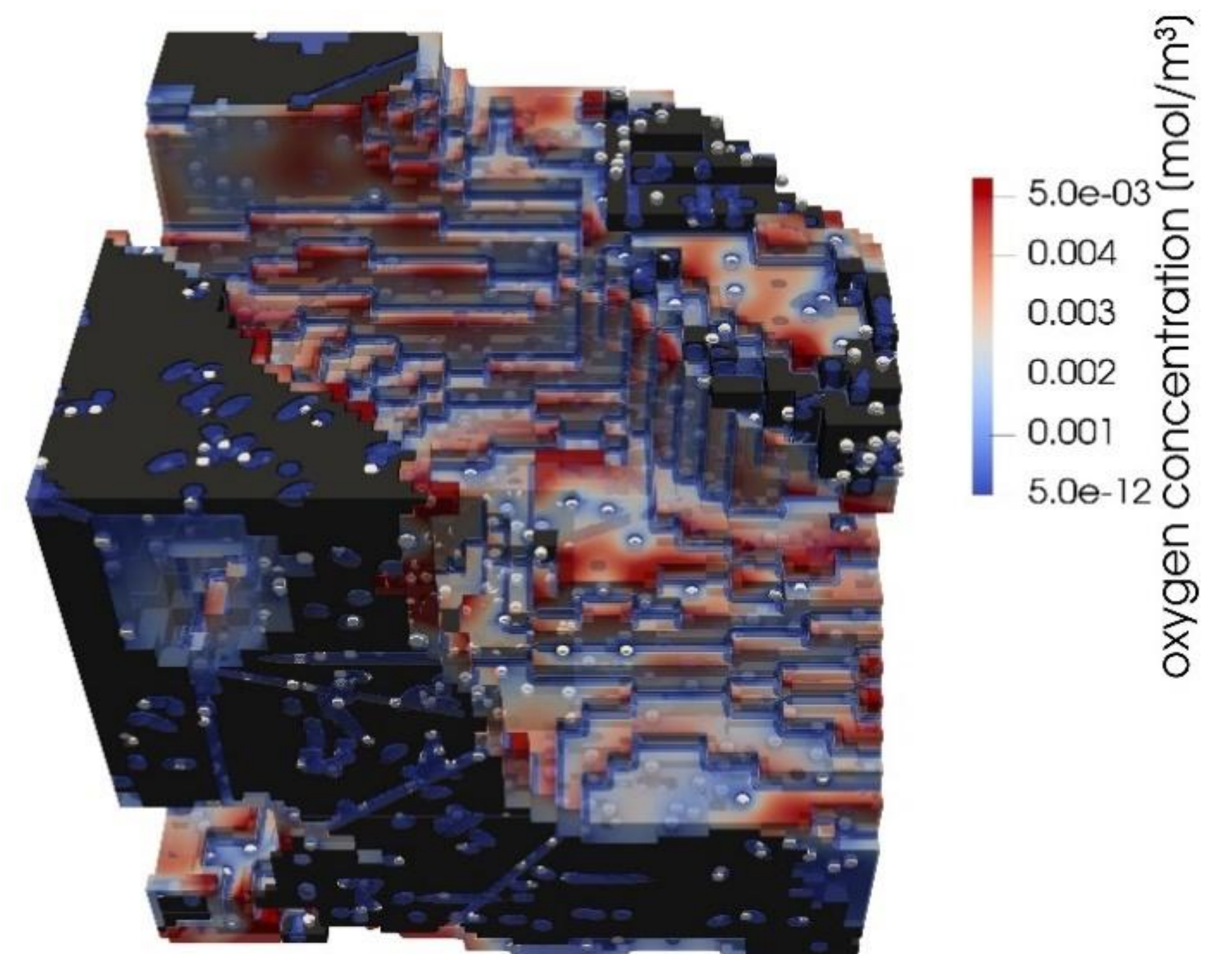
## Further Understanding Related to Transport limitations at High current density towards future ElectRodes for Fuel Cells



### Simulation of sub-micrometer CL operation with Lattice-Boltzmann Modeling

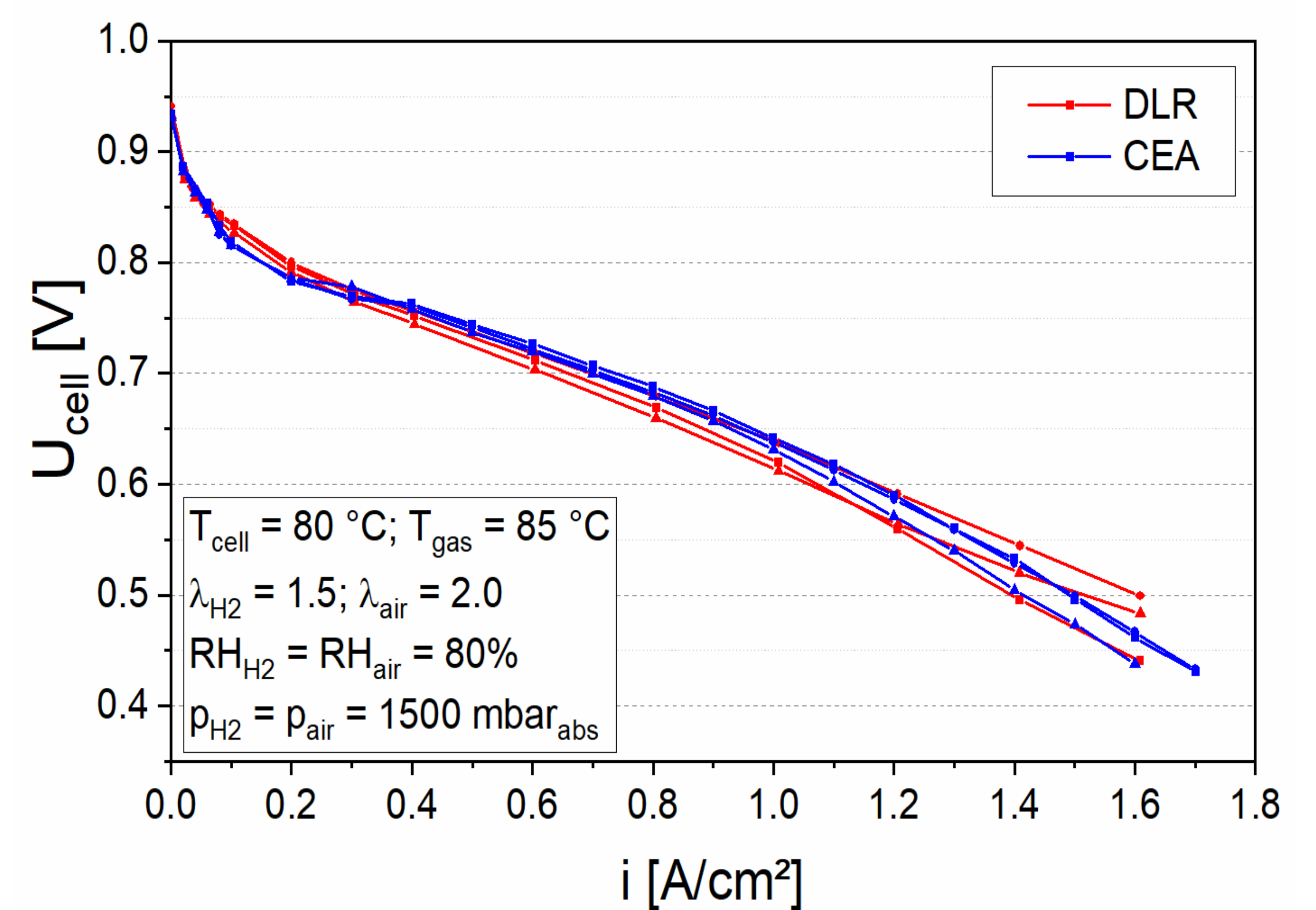
The aim of this task is to study the transport in the cathode catalyst layer (CCL) at the sub-micrometer scale and to identify the corresponding transport losses depending on the CCL sub-micrometer structure.

A Lattice Boltzmann model has been developed to simulate the oxygen transport within the complex CCL microstructures. This model includes the transport of oxygen within the gas phase, ionomer phase and liquid water phase as well as the interfaces between the different phases. The ORR is realized by a reactive boundary condition at the platinum surfaces. Realistic catalyst layer microstructures on the sub- $\mu\text{m}$  scale have been constructed, including the distribution of ionomer on the carbon support, construction of primary pores within the carbon as well as liquid water due to capillary condensation on the top right).

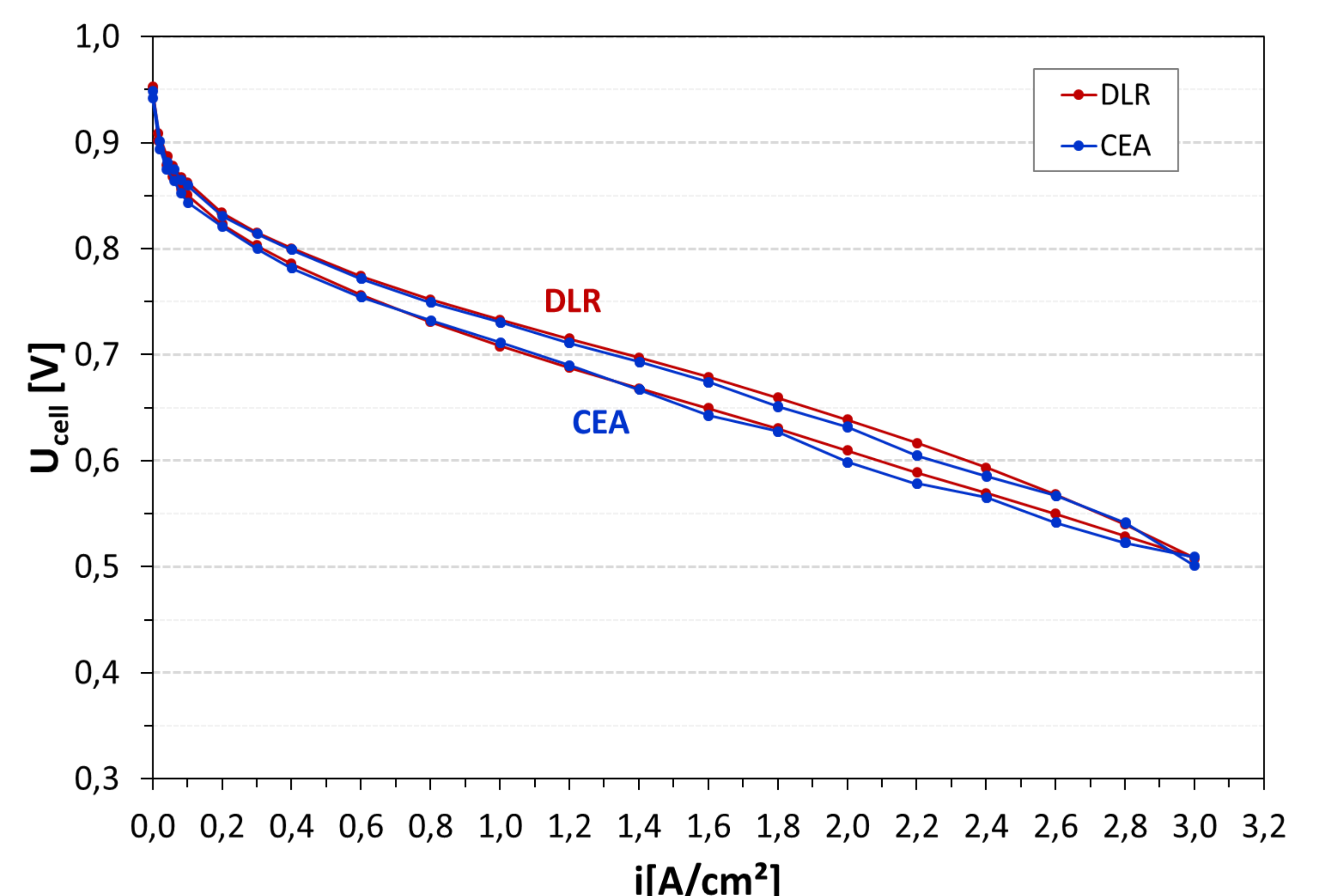


### Fuel cell characterisations

The reproducibility in the technical cells were examined using a standardized flow field design and the different conditions. The results using different test stations at DLR and at CEA provide similar performance and standard deviation between the different MEA batches. The presented results in on the top right show the comparability using the set 2 conditions – standard wet.



The reproducibility in the differential cells were examined using the set 3 conditions with fixed media flow according to a hydrogen and air stoichiometry of 32 at 3 A/cm<sup>2</sup> for 1 cm long channels. The flow field design was again standardized, but the channel length varied among the partners. The tests have shown that there are a few very important parameters to achieve comparability between the partners: (i) the flow field design has to be harmonized, (ii) differences in the setup (channel length, sensor position, cell cooling...) has to be identified and considered, and (iii) most important, the same MEA compression force has to be applied. Considering these parameters, enabled a very good comparability between the results measured in the different facilities as shown in on the bottom right.



# FURTHER-FC Newsletter #6

## Further Understanding Related to Transport limitations at High current density towards future Electrodes for Fuel Cells

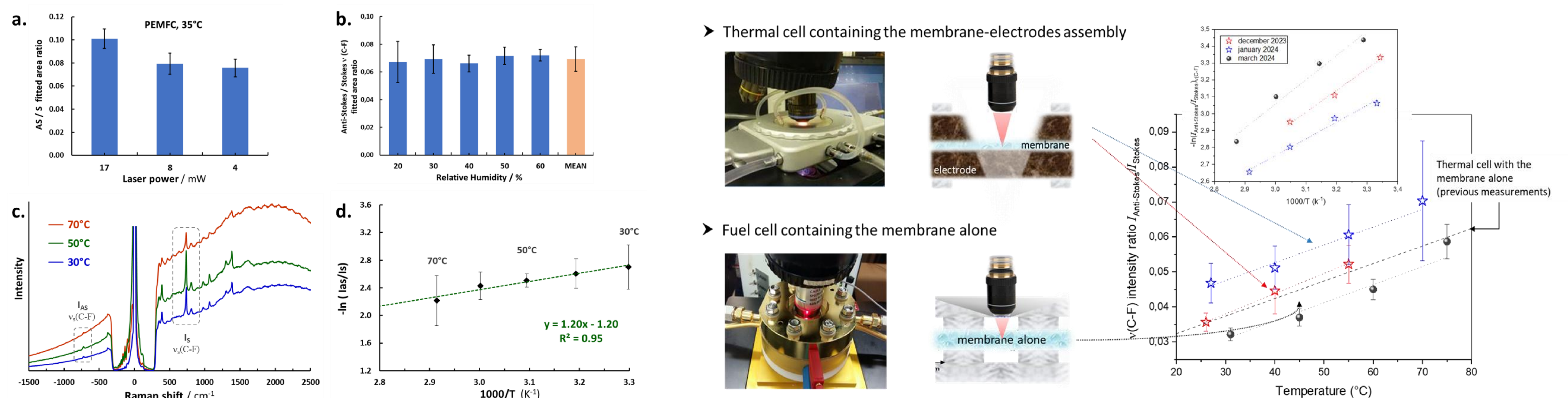


### Local conditions

For receiving local conditions close to the membrane-CL interface, a process had to be developed to burn the CCL using the laser. First tries lead to the deposition of most of the platinum included in the CCL onto the membrane. The procedure was then improved to limit the Pt deposition on the border of the circular area free from CCL. This new process consists in programming a spiral movement of the laser from the center to the outer borders. In addition, the composition of the atmosphere was changed for an oxygen-rich atmosphere to facilitate the carbon elimination by combustion. This new procedure can be considered definitive and allows to improve the signal-to-noise ratio when recording Raman spectra.

#### Calibration measurements

Calibration measurements which are necessary before operando Raman thermography have been completed. The conditions for in situ Raman measurements of the temperature were set by screening the influence of different parameters on the Anti Stokes to Stokes bands ratio. The power of the laser source showed to be the only parameter significantly affecting the measured ratio (below). This indicates that using the laser at full power may heat the membrane; thus, a reduced laser power of 8 mW was chosen for all measurements. The modification of the relative humidity showed no influence on the measured ratio, as well as for other parameters (detector sensibility, acquisition time, hole).



**Influence of (a) the laser power and (b) the relative humidity on the measured Anti-Stokes to Stokes intensity ratio. (c) Raman spectra of the membrane at different temperatures. (d) Calibration curve of the Anti-Stokes to Stokes intensity ratio versus temperature.**

The calibration of the Anti Stokes to Stokes ratio *versus* temperature was then carried out in the fuel cell under nitrogen, varying the temperature of the cell from 30°C to 70°C. The temperature was controlled *via* two Pt probes localized in the cathode and anode bipolar plates.

#### Operando measurements

A comprehensive set of measurements has been implemented in order to define the T/RH range accessible to the Raman thermometry technique. Operating T and RH are inter-related, mutually limiting and both depending on the current intensity delivered by the PEMFC. The maximum RH values that can be attained are determined by the specific FC design required for micro-Raman and limited by the occurring of water condensation. For example, at  $T = 35^\circ\text{C}$  and  $\text{RH}_{\text{outlet}} = 80\%$ , increasing  $I$  to values  $> 0.3 \text{ A}\cdot\text{cm}^{-2}$  induces water condensation in the MEA (particularly between the ribs), subsequently degrading the PEMFC performances. Increasing T but maintaining current and gases hydration constant at the inlets, induces water condensation at the PEMFE optical window hindering the acquisition of Raman spectra. Otherwise, the maximum/minimum attainable T/RH values depends on the membrane water content. Actually, the intensity of the Raman signal appears to be strongly affected by the membrane hydration. Increasing fluorescence is observed for membranes progressively less hydrated. This phenomenon leads to the gradual decrease of the signal to noise ratio and, thus, to the loss of the sensibility and precision of the Raman measurement. Concluding, the T/RH applicability domain of the Raman technique (with the specific cell and experimental set up of our laboratory) can be estimated as ranging from  $\text{RH}_{\text{min}} \sim 20\%$  at room temperature (30% at 35°C) up to  $\text{RH} = 80\%$  at  $T = 70^\circ\text{C}$ .

Some lack of reproducibility was observed for operando measurement, as well as the mismatch between the results from calibration data obtained with the membrane alone in the thermal cell and those from experiments with the MEA in the PEMFC under  $\text{N}_2$ . Then we completed our investigation by carrying out measurements, on the one hand, with the MEA in the thermal cell and, on the other, with the membrane alone in the PEMFC. The calibration lines thus obtained show similar slopes but stay offset from each other.

Concluding, the  $\mu$ -Raman thermography method as developed here is still affected by some lack of reliability when applied to the operating PEMFC. Two main reasons, concerning the spatial resolution and sensitivity limitations, can be hypothesized and stay to be solved:

- the membrane heating induced by the irradiation of the residual carbon remaining at the opposite side of the MEA after the electrode ablation by laser irradiation;
- the limited sensibility of the technique (i.e. too low signal to noise ratio) when applied to the complex PEMFC environment, arising from the way spectral data are processed.

# FURTHER-FC Newsletter #6

## Further Understanding Related to Transport limitations at High current density towards future ElectRodes for Fuel Cells



### GUIDELINES FOR NEW GENERATION OF PEMF MEA FOR AUTOMOTIVE APPLICATION

The final MEA of FURTHER-FC represents the MEA with the highest performance and lowest transport limitation as identified in the project. The performance and the durability in technical cell was significantly improved when HOPI is used as ionomer compared to D2020. The increase in performance with HOPI, especially under highly humid conditions, is attributed to a lower oxygen transport resistance, with at least a significant increase in  $O_2$  solubility. The decrease in ionomer poisoning of active sides of the catalyst can also be hypothesised, either due to less adsorption, especially of  $SO_3^-$  groups, on these catalytic sites, due to a difference in chemistry and/or in the distribution on the nm scale, or a more efficient distribution of the ionomer at the nano- and mesoscale resulting in less ionomer coverage on the catalyst. Furthermore, HOPI seems to increase the hydration of the CCL and increases thus the effective proton conductivity. The use of HOPI as ionomer in the CCL seems to suppress the degradation of the catalyst and potentially even of the catalyst support. This could be caused by differences in the ionomer coverage on the Pt catalyst, in the water content of the CCL or in the local pH value in the CCL. These parameters can have a direct impact on the Pt dissolution rate and on the carbon corrosion rate.

As well known, increased Pt loading is always beneficial for performance and durability due to the increased number of active catalyst sites and oxygen transport resistances. However, a higher Pt loading also increases the CCL thickness which is disadvantageous for the proton transport. This could require an increase of the Pt:C ratio for high Pt loadings. At the end, there is always a trade-off required between performance/durability and cost depending on the targeted application.

I:C ratio plays a crucial role for MEA performance and can directly impact the oxygen transport to the active catalyst sides as well as the water content and thus the proton transport in the CCL. The optimum of the I:C ratio depends on the operating conditions in the application. A low I:C ratio is beneficial for highly humidified conditions and operation at high current density to minimize electrode flooding. A high I:C ratio is beneficial for dry conditions to increase the proton conductivity of the CL and increase the performance at low current density. But this high I:C shows significant increase of the oxygen transport resistance and is therefore limited to operation at low current density. Furthermore, the optimum of the I:C ratio depends on the type of ionomer and used catalyst as well as the solvent for CCM manufacturing. Thereby, the formation of a dense ionomer layer at the MPL/CCL interface at high I:C ratios is very disadvantageous. This layer can be formed during CCL drying using the decal method (as applied in FURTHER-FC). It might be possible to avoid this layer by optimization of the used solvent and the applied drying parameters. Direct membrane deposition would result in an ionomer layer at CL/membrane interface what could be even beneficial, but this method can be challenging in other terms.

It is difficult to discuss the effect of the carbon support independently of other parameters like structure and porosity of the CCL, Pt particle size distribution and aggregation, ionomer distribution and water content in the CCL. GC use could require increased Pt loading for compensation of lower ECSA to achieve compatible performance over the entire current density range. But GC can improve performance at high current density due to lower  $O_2$  transport limitations. The resulting higher cost can be offset with increased durability of the carbon support depending on the application (e.g., automotive or heavy duty). Another potential trade-off would be the use of a mixture of Pt/GC and Pt/HSAC.

The use of higher Pt:C ratio and reduced CCL thickness is beneficial for MEA performance due to improved proton transport and for flooding conditions additionally due to improved oxygen transport. But this study was limited to GC as catalyst support and results might vary for HSAC and even higher Pt:C ratios, when Pt particle agglomeration shows negative impact on the ECSA. The use of a Pt:C ratio of 50% was beneficial from all point of views when compared to 30% as long as GC is used as carbon support. Only the potential challenges regarding ink dispersion and homogeneous preparation of very thin CCLs during MEA manufacturing should be mentioned.

The use of HOPI allowed to improve the performance in all the conditions, especially under highly humid conditions. In general, HOPI was identified to be very beneficial to improve performance and lifetime and as a highly interesting material for further MEA development. More research is needed to understand and optimize HOPI-based catalyst layers and the HOPI material from the chemical point of view. Thereby, the understanding of the catalyst layer structure is a key aspect. FURTHER-FC has also shown that the HOPI integration into catalyst layers can be challenging in terms of defect-free and reproducible layer deposition. Optimization of used solvents and coating procedures is needed to overcome these challenges.

The combination of HOPI and GC seems to be very challenging and requires potentially more optimization. The benefits of both materials could not be combined and the results enable the hypothesis that the distribution of the ionomer is very strongly depending of the used catalyst support.

For future development, we propose to use a mesoporous carbon support with a high degree of graphitization and an average particle diameter not exceeding 20 nm, with Pt nanoparticles located inside nanopores of about 5 to 10 nm in diameter, a few nm below the carbon surface. The aim is to obtain a highly homogeneous dispersion of the Pt nanoparticles within the volume of the CCL and to avoid direct contact of the ionomer with the catalyst, but as close as possible to the ionomer in order to reduce the path of the reactants ( $O_2$  and  $H^+$ ) towards the catalytic sites. The Pt particle size should be around 3 to 4 nm, distributed as homogeneously as possible within the volume of the CL. The graphitization improves the stability of the carbon.

HOPI or similar type of ionomer with an EW lower than 900 g/mol should be use. Most often cracks free and homogeneous CL are more difficult to manufacture with HOPI or with GC support especially for a targeted thickness not larger than 6  $\mu m$ , that would correspond to a Pt loading of about 0.2  $mg/cm^2$  for a Pt/C ratio equals to 0.5. The solvent plays a crucial role in obtaining homogeneous, cracks free and well performing CL.

The thickness of the CL must be reduced to the maximum by increasing Pt/C ratio. The difficulty is to avoid agglomeration of Pt nanoparticles when increasing this ratio. The agglomeration of Pt particles leads to more stable Pt electrocatalyst. However, it increases the local transport resistances. The porosity must be around 50 to 60%.

# FURTHER-FC Newsletter #6

## Further Understanding Related to Transport limitations at High current density towards future ElectRodes for Fuel Cells



### Conclusions

The FURTHER-FC project has enabled progress in our knowledge of the structure and operation of PEMFCs, and in particular the :

- High resolution geometrical data of the MPL structure and CL structure with ionomer distribution thanks to numerical analysis of the AI-assisted 3D reconstructed structure from FIB-SEM images.
- Computation of the transport properties of GDL and CL from 3D reconstructed structures
- Nanoscale organisation of the ionomer in the CL
- Water localisation in the CL
- Evolution of water content in the MEA with variation of total pressure
- Computation of the transport limitations at the nm scale within the pores and in the electrolyte
- Evidence of the limitations of LCA analyses and recommendations how to perform the measurements
- Evidence of the large impact of total pressure on the overall activity of the CCL
- Predictive performance model for a wide range of operating conditions taking into account Pt oxidation, water transport in ionomer and water filled nanopores and potential dependent ionomer adsorption on the catalytic sites based on the computed and measured parameters
- Evidence that  $H^+$ ,  $O_2$ ,  $H_2O$  transport and electrokinetic phenomena are difficult, if not impossible, to decouple and that experimental results can only be analysed using numerical physical models
- Evidence of enhanced durability with HOPI ionomer

### Acknowledgement

This project has received funding from the Fuel Cells and Hydrogen 2 Joint Undertaking under Grant Agreement No 875025. This Joint Undertaking receives support from the European Union's Horizon 2020 Research and Innovation programme, Hydrogen Europe and Hydrogen Europe Research.

Contact:  
[tobias.morawietz@hs-esslingen.de](mailto:tobias.morawietz@hs-esslingen.de)  
16/03/2025